IJAME
Int. J. of Applied Mechanics and Engineering, 2026, vol.31, No.1, pp.137-164
DOI: 10.59441/ijame/214148

UNSTEADY MHD 2- LIQUID HEAT TRANSMISSION PLASMA FLOW IN A ROTATING SYSTEM WITH HALL CURRENTS VIA PERMEABLE CONDUCTING PLATES

T. Linga Raju[1*] and Bonu Venkata Rao[2]
[1]Department of Engineering Mathematics, Andhra University, Visakhapatnam, Pin code: 530003 A.P., INDIA
[2]Basic Sciences, M.V.G.R. College of Engineering, Vizianagaram, A.P., INDIA
E-mail: tlraju45@yahoo.com & prof.tlraju@andhrauniversity.edu.in

A theoretical study is conducted on an unstable magneto hydrodynamic two-phase heat transfer plasma flow within a horizontal channel, which is bounded by conducting and permeable plates. The analysis takes place in a rotating frame of reference and includes the effect of Hall current. The regular perturbation approach determines the governing differential equations under the adopted conditions. The velocity and thermal distribution are visually resolved, and a parametric study is executed. Two fluid flow and heat transmission factors are affected by governing characteristics like as the porosity parameter, Hall parameter, Hartmann number, Taylor's number; and height, electrical, viscosity, and thermal conductivity ratios.

Key words: heat transfer, immiscible flow, rotating frame, Hall effect, conductive porous plates, perturbation method.

1. Introduction

MHD Plasma flows in a rotating framework have been a growing field of investigation with applications spanning several scientific and technological domains, such as astrophysics, geophysics and other allied areas. Examples include energy storage systems, solar receiving systems, plasma jets, electromagnetic pumps, fusion machines, MHD-power generators, and environmental geothermal systems.

The concept of the Hall Effect has attracted a lot of attention among the many useful physiognomies of MHD plasma flow. According to the research proposed by Cowling [1], Hall current effects in magnetized plasma become significant at very high magnetic field strengths. Hall currents are essential for improving energy productivity and system performance in a variety of technical applications as well as geophysical and astrophysical applications. Some of the applications include solar flares and magnetospheres, spacecraft propulsion, aerodynamic heating, plasma control generators, radio wave propagation, plasma jets, several power-generating systems and fusion reactors, MHD power plants, Hall accelerators, Hall effect thrusters, and creating thrust by ionizing and accelerating gas. Several researchers, namely Spitzer [2], Sato [3], Sutton and Sherman [4], Cramer and Shih [5], Ram [6], L. Raju and Rao [7], Takhar [8], Morley *et al.* [9], Hazem [10], Ghosh [11], Jha and Apere [12], Das and Deka [13], Sadia [14], Makinde *et al.* [15], and L. Raju *et al.* [16], have studied MHD liquid flows under the influence of a strong magnetic field with or without considering the rotation effects in different geometrical settings.

The suction or blowing significantly affects various industrial processes involving channel flow and heat transfer flow, as it can alter both flow dynamics and heat propagation. Similarly, it has been shown that magneto-hydrodynamic forces and Hall currents considerably affect MHD flow characteristics in channel flows with permeable plates. Due to the wide range of scientific and technological applications, several investigations have been documented in the literature, including works by Hazem [17], Ahmed and Goswami [18], Das *et al.* [19], Khaled and Jaber [20], Singh [21], L. Raju and Valli [22], Das *et al.* [23] and many more.

* To whom correspondence should be addressed

Likewise, major issues in geophysics, plasma physics, the petroleum industry, and other fields involve multi-layered or often two-layered flow environments in particular [24-27]. It is also well understood that fluid flows are normally unstable in nature. It is also useful in several practical situations to note that both immiscible liquids can carry electricity, especially when one is a strongly electrically conducting fluid compared to the other. Low-electrical-conductivity fluids are essential for minimizing power consumption while pumping fluid in flow meters and MHD pumps, among other applications (see Shail [28]). In a variety of technological, engineering, and industrial challenges, it is beneficial to determine the heat flow rate and the temperature distribution pattern as heat transfer progresses under unsteady motion in various geometrical environments. Designing cooling systems using geothermal reservoirs, liquid metals, petroleum, and subsurface energy transit, as well as MHD generators, accelerators, pumps, flow meters, polymer technology and crude oil purification, are among the essential applications. The study explores the behaviour of unsteady magneto hydrodynamic (MHD) two-fluid plasma flows in channels lined with electrically conducting porous plates. However, further study is required to determine how a Hall current affects these outcomes.

Considering the importance of such studies, the impact of resistivity and Hall Effect of a gas-liquid system was investigated by Kalra *et al.* [29]. L. Raju *et al.* [30] investigated the MHD two-phase thermal transfer flow with Hall current in a straight channel. Umavathi *et al.* [31] researched on heat transfer aspects of oscillatory Hartman type 2-fluidflow in a parallel channel. L. Raju and Valli [32] examined MHD unsteady 2-layered flow and thermal transmission via a parallel channel in a rotatory system. Sharma and Kalpana [33] researched the heat transfer of unsteady MHD two-phase flows through a channel. Sivakamini and Govindarajan [34] discussed unsteady magneto hydrodynamic flow of two immiscible fluids in a straight channel with chemical reaction. L. Raju [35] studied MHD heat transmission of two plasma flows in a parallel channel with Hall currents. L. Raju *et al.* [36] presented the flow pattern on the MHD 2-liquid plasma heat transfer flow with Hall currents between parallel plates. Later, L. Raju *et al.* [37] analysed the rotating heat transfer MHD two-plasma flow with Hall current. An unsteady MHD and heat transfer flow of two plasma liquids through a horizontal channel in a rotating system with Hall effect when the plates are composed of conducting plates was studied by L. Raju and Venkat [38]. Very recently, L. Raju and Venkat [39] performed the thermal transmission analysis of the influence of Hall on magneto hydrodynamic two plasmas unsteady flow between conducting plates with rotation.

To further enrich the background and relevance of this study, recent investigations on MHD heat transfer flows have contributed significant advances. Works such as those by Nikodijevic *et al.* [40] and Khader and Sharma [41] have explored related magneto hydrodynamic unsteady fluid flow and heat transfer phenomena, providing complementary insights relevant to the present research. Additionally, recent studies focusing on MHD convective heat and mass transfer flows in rotating systems, porous media, and numerical modelling approaches like studies [42-46] demonstrate ongoing interest and developments in the field also provide foundational context to this work. This integration of recent literature highlights the expanding landscape of MHD two-fluid flow analyses and underscores the novelty and applicability of the current investigation.

Provoked by the previously stated advances, this work investigates how Hall currents influence unsteady magneto hydrodynamic two-liquid heat transfer flow through a straight channel bounded by conducting permeable plates in a rotating system**.** An essential component of the current research is the insertion of wall porosity in the unsteady MHD two-fluid plasma flow model in to the existing literature; that is, this article is an extended work of [39]. The motivation for this study stems from the pressing need to understand and optimize the heat and fluid transport characteristics of plasma and electrically conducting fluids in complex, multiphase environments influenced by strong magnetic fields and rotational effects. Modern energy systems, such as fusion reactors, MHD generators, and advanced cooling applications, increasingly rely on the precise control of such flows, especially when Hall currents and wall permeability play essential roles in governing flow stability and thermal efficiency. Despite substantial prior research on single-phase or non-rotating MHD flows, the combined effects of Hall currents, rotation, and permeable conducting boundaries in two-phase systems remain underexplored, presenting challenges for both fundamental science and technology. By developing a robust theoretical model and systematic parametric

analysis, this work seeks to bridge these gaps, provide actionable insights for engineering design, and stimulate future innovations in energy extraction, propulsion, and high-temperature thermal management.

The present work has significant applications in advanced engineering and energy systems where precise control of heat and fluid flow is required under the influence of magnetic fields and rotational effects. In particular, the mathematical modelling and analysis are directly relevant to the design and optimization of cooling channels in nuclear fusion reactors, where plasma flows must be efficiently managed between conducting walls under strong magnetic and rotational fields. The insights gained are also be applicable to liquid metal flow in MHD generators and pumps, electromagnetic flow meters used in metallurgy, Hall effect thrusts for spacecraft propulsion, and boundary layer cooling of high-temperature components in power plants and aerospace systems. By capturing the combined influences of Hall currents, wall permeability, and rotation on heat transport, this research provides a foundation for improving energy efficiency, thermal management, and system stability in these cutting-edge technological applications.

2. Formulation of the problem and mathematical analysis

We consider the unsteady motion of a two-fluid magneto hydrodynamic (MHD) plasma flow with Hall current effects, driven by a uniform pressure gradient $-\frac{\partial p}{\partial x}$, in a channel bounded by two parallel porous conducting plates extending along the *x*- and *z*-directions. The study also includes the following considerations:

- The entire system is assumed to rotate with a constant angular velocity $\overline{\Omega}$ about the *y*-axis, which is perpendicular to the plates.
- A uniform suction velocity v_0 is applied at the boundaries, along with a constant magnetic field B_0 directed normal to the plates.
- The flow domain is divided into two regions: Region-I $(-h_2 \le y \le 0)$ and Region-II $(0 \le y \le h_1)$.
- The regions are occupied by two incompressible, electrically conducting, and immiscible fluids, each characterized by distinct viscosities (μ_1, μ_2), densities (ρ_1, ρ_2), electrical conductivities $(\sigma_{01}, \sigma_{02})$, and thermal conductivities (K_1, K_2).
- The bounding plates are maintained at constant temperatures and assumed to be infinitely long in both the *x*- and *z*-directions, so that all flow variables, except pressure, depend only on *y* and *t*.
- The interface separating the two fluids is considered perfectly flat, stress-free, and undisturbed.
- The induced magnetic field is neglected under the assumption that the magnetic Reynolds number is sufficiently small.

Based on these assumptions and guided by insights from established research, the proposition involves the following governing equations for an unsteady motion explicitly accounting for Hall currents and rotation subject to the relevant boundary and interface conditions, aligning with the foundational work on hydro-magnetic steady flows by Spitzer [47], Sato [3] and L. Raju [35].

Governing equations of motion:

$$\rho\left[\frac{\partial \overline{V}}{\partial t}+\left(\overline{V}\cdot\nabla\right)\overline{V}\right]+2\rho\overline{\Omega}\times\overline{\mathrm{V}}=-\nabla p+\mu\nabla^2\overline{V}+\left(\overline{J}\times\overline{B}\right). \tag{2.1}$$

Current equation:

$$\overline{E}+\overline{V}\times\overline{B}+\overline{E_e}-\frac{c}{en}\overline{J}\times\overline{B}-\frac{\overline{J}}{\sigma_0}=0. \tag{2.2}$$

Energy conservation equation:

$$\rho\, c_p\left[\frac{\partial T}{\partial t}+\left(\overline{V}\cdot\nabla\right)T\right]=K\,\nabla^2 T+\phi+\left(\overline{J}^2/\sigma_0\right). \tag{2.3}$$

Continuity equation for incompressible fluid flow:

$$\nabla\cdot\overline{V}=0\,. \tag{2.4}$$

The governing flow equations are formulated considering the velocity field $\overline{V_i}=(u_i,v_0,w_i)$, magnetic field $\overline{B}=(0,B_0,0)$, angular velocity $\overline{\Omega}=(0,\Omega,0)$, current density is given as $\overline{J_i}=(J_{ix},0,J_{iz})$, while the electric field is represented as $\overline{E_i}=(\mathrm{E}_{ix},0,E_{iz})$ and $J_i^2=J_{ix}^2+J_{iz}^2$, $i=1,2$; in both lower and upper regions using the aforementioned assumptions and studies like as in [3, 22, 35 and 39]. To non-dimensionalize the governing equations, the following set of transformations is applied.
For the two liquids: $i=1,2$:

$$\begin{gathered}
y_i^*=\frac{y_i}{h_i},\quad u_p=-\frac{h_i^2}{\mu_i}\frac{\partial p}{\partial x},\quad u_i^*=\frac{u_2}{u_p},\quad w_i^*=\frac{w_2}{u_p},\quad t^*=\frac{\mu_i t}{\rho_i h_i^2},\quad \omega^*=\frac{\omega h_i^2\rho_i}{\mu_i},\\
m_{ix}=\frac{E_{ix}}{B_0u_p},\quad m_{iz}=\frac{E_{iz}}{B_0u_p},\quad I_{ix}=\frac{J_{ix}}{\sigma_{0i}B_0u_p},\quad I_{iz}=\frac{J_{iz}}{\sigma_{0i}B_0u_p},\quad M=B_0h_1\sqrt{\frac{\sigma_{01}}{\mu_1}},\\
K=h_1\sqrt{\frac{\Omega}{\nu_1}},\quad \lambda=\frac{h_1\rho_1v_0}{\mu_1},\quad \beta=\frac{K_1}{K_2},\quad \theta_i=\frac{T_i-T_{wi}}{\left(u_p^2\mu_1/K_i\right)},\\
\sigma_0=\frac{\sigma_{01}}{\sigma_{02}},\quad \sigma_1=\frac{\sigma_{12}}{\sigma_{11}},\quad \sigma_2=\frac{\sigma_{22}}{\sigma_{21}},\quad \frac{1}{1+m^2}=\frac{\sigma_{11}}{\sigma_{01}},\quad m=\frac{\omega_e}{\left(\frac{1}{\tau}+\frac{1}{\tau_e}\right)}.
\end{gathered} \tag{2.5}$$

Although the channel side plates are composed of conducting material and are intended to be short-circuited by an external conductor, the induced electric current is expected to flow out of the channel. There is no electric potential between the channel plates at that moment. We also have $m_{ix}=0,\ m_{iz}=0$ if we accept no electric field in the *x* and *z* axes (as in Sato [3] and L. Raju [35]). Due to the utilisation of transforms (2.5) and disregarding the asterisks for simplicity, the dimensionless governing equations and conditions in the two regions for instance of conducting porous plates, take the following form.

Region-I

$$\frac{\partial u_1}{\partial t}+\lambda\frac{\partial u_1}{\partial y}-\frac{\partial^2 u_1}{\partial y^2}+\frac{M^2u_1}{1+m^2}+\frac{M^2mw_1}{1+m^2}-L_1=-2K^2w_1, \tag{2.6}$$

$$\frac{\partial w_1}{\partial t}+\lambda\frac{\partial w_1}{\partial y}-\frac{\partial^2 w_1}{\partial y^2}+\frac{M^2w_1}{1+m^2}-\frac{M^2mu_1}{1+m^2}-L_2=2K^2u_1, \tag{2.7}$$

$$\frac{d\theta_1}{dt}=\frac{1}{P_{r1}}\frac{\partial^2\theta_1}{\partial y^2}+\lambda\frac{\partial\theta_1}{\partial y}+\left\{\left(\frac{\partial u_1}{\partial y}\right)^2+\left(\frac{\partial w_1}{\partial y}\right)^2\right\}+M^2{I_1}^2, \tag{2.8}$$

$$I_{1x}=\frac{mu_1}{1+m^2}-\frac{w_1}{1+m^2}-\frac{s}{M^2}\frac{m}{1+m^2}, \tag{2.9}$$

$$I_{1z}=\frac{u_1}{1+m^2}+\frac{mw_1}{1+m^2}+\frac{s}{M^2}\left(1-\frac{m}{1+m^2}\right) \tag{2.10}$$

and

$${I_1}^2={I_{1x}}^2+{I_{1z}}^2.$$

Region-II

$$\frac{\partial u_2}{\partial t}+\rho\alpha h\lambda\frac{\partial u_2}{\partial y}-\frac{\partial^2 u_2}{\partial y^2}+\frac{\alpha\sigma_1 h^2M^2u_2}{1+m^2}+\frac{m\alpha\sigma_2 h^2M^2w_2}{1+m^2}-L_3\alpha h^2=-2\rho\alpha h^2K^2w_2, \tag{2.11}$$

$$\frac{\partial w_2}{\partial t}+\rho\alpha h\lambda\frac{\partial w_2}{\partial y}-\frac{\partial^2 w_2}{\partial y^2}+\frac{\alpha\sigma_1 h^2M^2w_2}{1+m^2}-\frac{m\alpha\sigma_2 h^2M^2u_2}{1+m^2}-L_4\alpha h^2=2\rho\alpha h^2K^2u_2, \tag{2.12}$$

$$\frac{d\theta_2}{dt}=\frac{1}{P_{r2}}\frac{d^2\theta_2}{dy^2}+h\rho\alpha\lambda\frac{d\theta_2}{dy}+\frac{\beta}{\alpha}\left\{\left(\frac{du_2}{dy}\right)^2+\left(\frac{dw_2}{dy}\right)^2\right\}+h^2\sigma\beta M^2{I_2}^2, \tag{2.13}$$

$$I_{2x}=\frac{m\sigma_0\sigma_2u_2}{1+m^2}-\frac{\sigma_0\sigma_1w_2}{1+m^2}-\frac{s{\sigma_0}^2\sigma_2}{M^2}\frac{m}{1+m^2}, \tag{2.14}$$

$$I_{2z}=\frac{\sigma_0\sigma_1u_2}{1+m^2}+\frac{m\sigma_0\sigma_2w_2}{1+m^2}+\left(1-\frac{\sigma_0\sigma_1}{1+m^2}\right)\frac{s\sigma_0}{M^2} \tag{2.15}$$

and

$${I_2}^2={I_{2x}}^2+{I_{2z}}^2.$$

Where,

$$L_1=1-\frac{m^2s}{1+m^2},\quad L_2=\frac{-ms}{1+m^2},\quad L_3=1-\left(1-\frac{\sigma_0\sigma_1}{1+m^2}\right)s,\quad L_4=\frac{-\sigma_0\sigma_2ms}{1+m^2}.$$

Boundary and interface conditions on velocity are:

$$\begin{aligned}&\text{At the upper plate } y=1:\ u_1=0 \text{ when } t\le 0 \text{ and } =\varepsilon\cos\omega t \text{ when } t>0,\\ &\qquad\qquad\qquad\qquad w_1=0 \text{ when } t\le 0 \text{ and } =\varepsilon\cos\omega t \text{ when } t>0.\end{aligned} \tag{2.16}$$

$$\text{At the lower plate } y=-1:\ u_2=0 \text{ and } w_2=0. \tag{2.17}$$

$$\text{At the interface } y = 0: u_1 = u_2,\ w_1 = w_2,\ \frac{\partial u_1}{\partial y} = \left(1/\alpha h\right)\frac{\partial u_2}{\partial y},\ \text{and } \frac{\partial w_1}{\partial y} = \left(1/\alpha h\right)\frac{\partial w_2}{\partial y}. \quad (2.18)$$

The conditions on temperature are given by

$$\theta_1 = 0 \text{ at } y = 1 \text{ and } \theta_2 = 0 \text{ at } y = -1. \quad (2.19)$$

$$\text{At the interface } y = 0: \theta_1 = \theta_2 \text{ and } \frac{d\theta_1}{dy} = \frac{1}{h\beta}\frac{d\theta_2}{dy}. \quad (2.20)$$

In all the above equations, the fluid measures in the upper and lower areas are indicated by subscripts *1* and *2* equations. The initial and secondary velocity profiles refer to aspects of velocity along the ***x-*** and ***z-*** directions of the two fluid layers, which are denoted by u_1, u_2, w_1, w_2. The *x*- and *z*-directional current densities and electric field, respectively, are represented by J_{ix}, J_{iz} and $E_{ix}, E_{iz}, i = 1,2$. The quantity 's' stands for the ratio of electron pressure p_e to the overall pressure p. The quantities T_1 and T_2 represent the temperature of two fluids. The notations σ_{11}, σ_{12} and σ_{21}, σ_{22} denote the modified conductivities. The quantity u_p stands for characteristic length. The symbol C_{pi} stands for specific heat at constant pressure. The quantity ϕ is viscous dissipation term in the energy equation. The notation *M* is the Hartmann number, *m*: Hall parameter, *K*: rotation parameter (Taylor number), λ: porous parameter, *h*: height ratio, σ_0: viscosity ratio, α: electrical conductivity ratio and β: the thermal conductivity ratio.

The porous parameter λ specify that a positive λ corresponds to porous plates that allow fluid flow through them, which is the physical scenario of interest. Porosity greater than zero means the plates have some permeability, enabling suction or blowing effects that influence the magneto hydrodynamic two-fluid plasma flow and heat transfer. Non-porous plates as limit case: When $\lambda = 0$, the plates become impermeable (non-porous), and the problem reduces to the classical case without porosity effects. This case has been studied previously (e.g., in reference cited in the manuscript). The current study extends that by including porous effects, so it focuses on $\lambda > 0$ to explore new physics introduced by permeability. Model consistency and mathematical validity: negative values of λ would imply non-physical inverse permeability or act as impermeable with reversed flow, which is not meaningful in the context of the proposed model and boundary conditions. Hence, the restriction $\lambda > 0$ is both physically realistic and mathematically consistent with the model's focus on flow through permeable conducting plates.

The boundary conditions at the interface between two immiscible, electrically conducting fluids are fundamental to the mathematical formulation and physical understanding of MHD plasma flow. Physically, these conditions ensure: For viscous fluids, the movement at the boundary follows the no-slip condition, meaning the fluid in direct contact with a rigid surface matches the velocity of that surface. If the boundary is fixed, the velocity at the wall is zero, while for a moving plate; it equals the plate's velocity. This rule applies similarly to other velocity components such as '*v*' and '*w*' as the case may be. At the interface between two immiscible fluids, both velocity and shear stress are assumed to remain continuous across the boundary.

In terms of heat transfer, isothermal boundary conditions are often applied, assuming the solid surfaces in contact with the fluid have infinite thermal conductivity and heat capacity. Under these conditions, the fluid temperature at the surface matches that of the boundary. At interfaces between two immiscible fluids, both temperature and heat flux are considered continuous, ensuring smooth thermal behaviour across the junction.

Collectively, these interface conditions reflect fundamental physical principles–conservation of mass, momentum, and energy–and are essential for accurate modelling of two-phase MHD flows, where realistic interaction between fluids is key to predicting system behaviour under electromagnetic, rotational, and porous wall effects.

3. Solution scheme

The Eqs (2.6, 2.7, 2.11 and 2.12) and Eqs (2.9, 2.10, 2.14, and 2.15) must first be solved under the boundary and interface conditions (2.16 to 2.18) for the velocity distributions and current distributions in order to determine the solution for temperature in the two liquid regions. Following that the velocity and current distributions are used to solve the Eqs (2.8) and (2.13) under the conditions (2.19 to 2.20). These coupled partial differential equations are unsolvable to closed-form solutions. However, by considering the following two-term series, they can be reduced to the ordinary linear differential equations. It is elaborate on the regular perturbation method, its justification for this type of nonlinear, unsteady flow system, and a step-by-step outlay of the analytical approach used for deriving the solutions.

$$u_1(y,t) = u_{01}(y) + \varepsilon \cos \omega t\, u_{11}(y), \quad w_1(y,t) = w_{01}(y) + \varepsilon \cos \omega t\, w_{11}(y), \tag{3.1}$$

$$u_2(y,t) = u_{02}(y) + \varepsilon \cos \omega t\, u_{12}(y), \quad w_2(y,t) = w_{02}(y) + \varepsilon \cos \omega t\, w_{12}(y), \tag{3.2}$$

$$\theta_1(y,t) = \theta_{01}(y) + (\varepsilon \cos \omega t)\ \theta_{11}(y), \quad \theta_2(y,t) = \theta_{02}(y) + (\varepsilon \cos \omega t)\ \theta_{12}(y) \tag{3.3}$$

where, $u_{11}(y)$, $u_{12}(y)$, $w_{11}(y)$, $w_{12}(y)$ and $\theta_{11}(y), \theta_{12}(y)$ are the related time dependent parts while $u_{01}(y)$, $u_{02}(y)$, $w_{01}(y)$, $w_{02}(y)$ and $\theta_{01}(y)$, $\theta_{02}(y)$ are the solutions for the velocity and temperature in the two-liquid zones under the steady part to the problem of investigation.

Utilizing the expressions (3.1to 3.3) into the Eqs (2.6, 2.7, 2.8 and 2.11, 2.12, 2.13) and then obtain the following linear differential equations. Subsequently, they are solved analytically in using the interface and boundary conditions. The analytic solutions for transient-time dependent and steady parts are obtained separately to acquire the solutions of velocity and temperature fields in 2-liquid zones for instance of porous conducting plates.

Region-I

$$\frac{d^2 q_{01}}{dy^2} - \lambda \frac{dq_{01}}{dy} - b_2 q_{01} = b_3, \tag{3.4}$$

$$\frac{d^2 q_{11}}{dy^2} - \lambda \frac{dq_{11}}{dy} - (b_2 - \omega \tan \omega t)\, q_{11} = 0, \tag{3.5}$$

$$\frac{1}{P_{r1}} \frac{d^2 \theta_{01}}{dy^2} + \lambda \frac{d\theta_{01}}{dy} = -\left(\frac{dq_{01}}{dy} \frac{d\bar{q}_{01}}{dy} \right) - \left(b_{25} \bar{b}_{25} q_{01} \overline{q_{01}} + q_{01} b_{25} \overline{b_{26}} + \overline{q_{01}}\ \overline{b_{25}}\ b_{26} + b_{26} \overline{b_{26}} \right) M^2 \tag{3.6}$$

$$\begin{aligned} &\frac{1}{P_{r1}} \frac{d^2 \theta_{11}}{dy^2} + \lambda \frac{d\theta_{11}}{dy} + \omega \tan \omega t\ \theta_{11} = -\left(\frac{dq_{11}}{dy} \frac{d\bar{q}_{01}}{dy} - \frac{dq_{01}}{dy} \frac{d\bar{q}_{11}}{dy} \right) - \varepsilon \cos \omega t \left(\frac{dq_{11}}{dy} \frac{d\bar{q}_{11}}{dy} \right) + \\ &- \left(q_{01} \overline{q_{11}}\ \overline{b_{25}}\ b_{25} + b_{25} \overline{b_{25}}\, \overline{q_{01}}\ q_{11} + \varepsilon \cos \omega t\ b_{25} \overline{b_{25}}\ q_{11} \overline{q_{11}} + q_{11} b_{25} \overline{b_{26}} + b_{26} \overline{b_{25}}\ \overline{q_{11}} \right) M^2. \end{aligned} \tag{3.7}$$

Region-II

$$\frac{d^2 q_{02}}{dy^2} - \lambda_1 \frac{dq_{02}}{dy} - b_5 q_{02} = b_6 , \tag{3.8}$$

$$\frac{d^2 q_{12}}{dy^2} - \lambda_1 \frac{dq_{12}}{dy} - \left(b_5 - \omega \tan \omega t\right) q_{12} = 0 , \tag{3.9}$$

$$\frac{1}{P_{r2}} \frac{d^2 \theta_{02}}{dy^2} + h \rho \alpha \lambda \frac{d\theta_{02}}{dy} = -\left(\frac{dq_{02}}{dy} \frac{d\bar{q}_{02}}{dy} \right) \frac{\beta}{\alpha} - \\ + \left(b_{23} \overline{b_{23}}\, \overline{q_{02}}\, q_{02} + \overline{b_{27}}\, b_{23} q_{02} + b_{27} \overline{b_{23}}\, \overline{q_{02}} + b_{27} \overline{b_{27}} \right) h^2 M^2 \sigma \beta, \tag{3.10}$$

$$\frac{1}{P_{r2}} \frac{d^2 \theta_{12}}{dy^2} + h \rho \alpha \lambda \frac{d\theta_{12}}{dy} + \omega \tan \omega t\, \theta_{12} = -\left\{ \left(\frac{dq_{02}}{dy} \frac{d\bar{q}_{12}}{dy} + \frac{dq_{12}}{dy} \frac{d\bar{q}_{02}}{dy} \right) + \right. \\ \left. + \varepsilon \cos \omega t \left(\frac{dq_{12}}{dy} \frac{d\bar{q}_{12}}{dy} \right) \right\} \frac{\beta}{\alpha} - \left\{ \overline{b_{23}} b_{23} q_{02} \overline{q_{12}} + \overline{b_{23}}\, b_{23} q_{12} \overline{q_{02}} + \right. \\ \left. + \varepsilon \cos \omega t \left(\overline{b_{23}}\, b_{23}\, q_{12} \overline{q_{12}} \right) + \overline{b_{27}}\, b_{23} q_{12} + \overline{b_{23}}\, b_{27}\, \overline{q_{12}} \right\} h^2 M^2 \sigma \beta. \tag{3.11}$$

The boundary conditions for steady state are given by

$$\text{At } y = 1 : \; q_{01} = 0 \text{ and at } y = -1 : \; q_{02} = 0. \tag{3.12}$$

$$\text{At the interface } y = 0 : q_{01}(0) = q_{02}(0), \quad \frac{dq_{01}}{dy} = \frac{1}{\alpha h} \frac{dq_{02}}{dy}, \tag{3.13}$$

$$\theta_{01}(1) = 0, \quad \theta_{02}(-1) = 0 . \tag{3.14}$$

$$\text{At } y = 0 : \; \theta_{01}(0) = \theta_{02}(0) \text{ and } \frac{d\theta_{01}}{dy} = \frac{1}{\beta h} \frac{d\theta_{02}}{dy}. \tag{3.15}$$

Transient time dependent part:

$$q_{11}(1) = 0 \text{ and } q_{12}(-1) = 0. \tag{3.16}$$

$$q_{11}(0) = q_{12}(0) \text{ and } \frac{dq_{11}}{dy} = \frac{1}{\alpha h} \frac{dq_{12}}{dy} \text{ at } y = 0, \tag{3.17}$$

$$\theta_{11}(1) = 0, \quad \theta_{12}(-1) = 0 , \tag{3.18}$$

$$\theta_{11}(0)=\theta_{12}(0) \quad \text{and} \quad \frac{d\theta_{11}}{dy}=\frac{1}{\beta h}\frac{d\theta_{12}}{dy} \quad \text{at interface } y=0. \tag{3.19}$$

By solving the equations from (3.4 to 3.11) with the help of the conditions (3.12 to 3.19), the following equations were obtained for both the velocity and thermal fields in the two zones, as well as the rates of thermal transmission coefficients at the conducting porous walls:

Region-I

$$q_1(y,t)=q_{01}(y)+\varepsilon\cos\omega t\, q_{11}(y)=B_1e^{b_7y}+B_2e^{b_8y}-b_9+\varepsilon\cos\omega t\left(B_5e^{b_{10}y}+B_6e^{b_{11}y}\right), \tag{3.20}$$

$$\begin{aligned}\theta_1(y,t) &= \theta_{01}(y)+(\varepsilon\cos\omega t)\,\theta_{11}(y)= B_9+B_{10}e^{-\lambda_2}y+b_{28}e^{(b_7+\overline{b_7})y}+b_{29}e^{(b_7+\overline{b_8})y}+\\ &b_{30}e^{(b_8+\overline{b_7})y}+b_{31}e^{(b_8+\overline{b_8})y}+b_{32}e^{b_7y}+b_{33}e^{b_8y}+b_{34}e^{\overline{b_7}y}+b_{35}e^{\overline{b_8}y}+b_{36}+\varepsilon\cos\omega t\\ &\left\{B_{13}e^{b_{37}y}+B_{14}e^{b_{38}y}+b_{39}e^{(b_{10}+\overline{b_{10}})y}+b_{40}e^{(b_{10}+\overline{b_{11}})y}+b_{41}e^{(b_{11}+\overline{b_{10}})y}+b_{42}e^{(b_{11}+\overline{b_{11}})y}+\right.\\ &b_{43}e^{(b_7+\overline{b_{10}})y}+b_{44}e^{(b_7+\overline{b_{11}})y}+b_{45}e^{(b_8+\overline{b_{10}})y}+b_{46}e^{(b_8+\overline{b_{11}})y}+b_{47}e^{(b_{10}+\overline{b_7})y}+\\ &\left.b_{48}e^{(b_{10}+\overline{b_8})y}+b_{49}e^{(b_{11}+\overline{b_7})y}+b_{50}e^{(b_{11}+\overline{b_8})y}+b_{51}e^{\overline{b_{10}}y}+b_{52}e^{\overline{b_{11}}y}+b_{53}e^{b_{10}y}+b_{54}e^{b_{11}y}\right\},\end{aligned} \tag{3.21}$$

$$\begin{aligned}Nu_1 &= -\left(\frac{\partial\theta_1}{\partial y}\right)_{\text{at } y=1}=-\left\{-\lambda_2B_{10}e^{-\lambda_2}+b_{28}(b_7+\overline{b_7})e^{(b_7+\overline{b_7})}+b_{29}(b_7+\overline{b_8})e^{(b_7+\overline{b_8})}+\right.\\ &+b_{30}(b_8+\overline{b_7})e^{(b_8+\overline{b_7})}+b_{31}(b_8+\overline{b_8})e^{(b_8+\overline{b_8})}+b_{32}b_7e^{b_7}+b_{33}b_8e^{b_8}+b_{34}\overline{b_7}e^{\overline{b_7}}+\\ &+b_{35}\overline{b_8}e^{\overline{b_8}}+\varepsilon\cos\omega t\left[B_{13}b_{37}e^{b_{37}}+B_{14}b_{38}e^{b_{38}}+b_{39}(b_{10}+\overline{b_{10}})e^{(b_{10}+\overline{b_{10}})}+\right.\\ &+b_{40}(b_{10}+\overline{b_{11}})e^{(b_{10}+\overline{b_{11}})}+b_{41}(b_{11}+\overline{b_{10}})e^{(b_{11}+\overline{b_{10}})}+b_{42}(b_{11}+\overline{b_{11}})e^{(b_{11}+\overline{b_{11}})}+\\ &+b_{43}(b_7+\overline{b_{10}})e^{(b_7+\overline{b_{10}})}+b_{44}(b_7+\overline{b_{11}})e^{(b_7+\overline{b_{11}})}+b_{45}(b_8+\overline{b_{10}})e^{(b_8+\overline{b_{10}})}+\\ &+b_{46}(b_8+\overline{b_{11}})e^{(b_8+\overline{b_{11}})}+b_{47}(b_{10}+\overline{b_7})e^{(b_{10}+\overline{b_7})}+b_{48}(b_{10}+\overline{b_8})e^{(b_{10}+\overline{b_8})}+\\ &+b_{49}(b_{11}+\overline{b_7})e^{(b_{11}+\overline{b_7})}+b_{50}(b_{11}+\overline{b_8})e^{(b_{11}+\overline{b_8})}+b_{51}\overline{b_{10}}e^{\overline{b_{10}}}+b_{52}\overline{b_{11}}e^{\overline{b_{11}}}+\\ &\left.\left.+b_{53}b_{10}e^{b_{10}}+b_{54}b_{11}e^{b_{11}}\right]\right\}.\end{aligned} \tag{3.22}$$

Region-II

$$\begin{aligned}&q_2\ (y,t)=q_{02}\ (y)+\varepsilon\cos\omega t\ q_{12}\ (y)=\\ &=B_3e^{b_{12}y}+B_4e^{b_{13}y}-b_{14}+\varepsilon\cos\omega t\left(B_7e^{b_{15}y}+B_8e^{b_{16}y}\right),\end{aligned} \tag{3.23}$$

$$\theta_2(y,t)=\theta_{02}(y)+(\varepsilon\cos\omega t)\ \theta_{12}(y)=B_{11}+B_{12}e^{-\lambda_3 y}+b_{55}e^{(b_{12}+\overline{b_{12}})y}+$$
$$+b_{56}e^{(b_{12}+\overline{b_{13}})y}++b_{57}e^{(b_{13}+\overline{b_{12}})y}+b_{58}e^{(b_{13}+\overline{b_{13}})y}+b_{59}e^{\overline{b_{12}}y}+b_{60}e^{\overline{b_{13}}y}+b_{61}e^{b_{21}y}+$$
$$+b_{62}e^{b_{13}y}+b_{63}++\varepsilon\cos\omega t\Big[B_{15}e^{b_{80}y}+B_{16}e^{b_{81}y}+b_{64}e^{(b_{15}+\overline{b_{15}})y}+b_{65}e^{(b_{15}+\overline{b_{16}})y}+$$
$$+b_{66}e^{(b_{16}+\overline{b_{15}})y}++b_{67}e^{(b_{16}+\overline{b_{16}})y}+b_{68}e^{(b_{15}+\overline{b_{12}})y}+b_{69}e^{(b_{15}+\overline{b_{13}})y}+b_{70}e^{(b_{16}+\overline{b_{13}})y}+$$
$$+b_{71}e^{(b_{16}+\overline{b_{12}})y}++b_{72}e^{(b_{12}+\overline{b_{15}})y}+b_{73}e^{(b_{13}+\overline{b_{15}})y}+b_{74}e^{(b_{12}+\overline{b_{16}})y}+b_{75}e^{(b_{13}+\overline{b_{16}})y}+$$
$$+b_{76}e^{\overline{b_{15}}y}+b_{77}e^{\overline{b_{16}}y}+b_{78}e^{b_{15}y}+b_{79}e^{b_{16}y}\Big], \tag{3.24}$$

$$Nu_2=\frac{1}{\beta h}\left(\frac{\partial\theta_2}{\partial y}\right)_{at\ y\ =\ -1}=-\frac{1}{\beta h}\Big\{-\lambda_3 B_{12}e^{-\lambda_3}+b_{55}(b_{12}+\overline{b_{12}})e^{-(b_{12}+\overline{b_{12}})}+$$
$$+b_{56}(b_{12}+\overline{b_{13}})e^{-(b_{12}+\overline{b_{13}})}+b_{57}(b_{13}+\overline{b_{12}})e^{-(b_{13}+\overline{b_{12}})}+b_{58}(b_{13}+\overline{b_{13}})e^{-(b_{13}+\overline{b_{13}})}+$$
$$+b_{59}\overline{b_{12}}e^{-\overline{b_{12}}}+b_{60}\overline{b_{13}}e^{-\overline{b_{13}}}+b_{61}b_{21}e^{-b_{21}}++b_{62}b_{13}e^{-b_{13}}+\varepsilon\cos\omega t\Big[B_{15}b_{80}e^{-b_{80}}+$$
$$+B_{16}b_{81}e^{-b_{81}}+b_{64}(b_{15}+\overline{b_{15}})e^{-(b_{15}+\overline{b_{15}})}+b_{65}(b_{15}+\overline{b_{16}})e^{-(b_{15}+\overline{b_{16}})}+$$
$$+b_{66}(b_{16}+\overline{b_{15}})e^{-(b_{16}+\overline{b_{15}})}+b_{67}(b_{16}+\overline{b_{16}})e^{-(b_{16}+\overline{b_{16}})}+b_{68}(b_{15}+\overline{b_{12}})e^{-(b_{15}+\overline{b_{12}})}+$$
$$+b_{69}(b_{15}+\overline{b_{13}})e^{-(b_{15}+\overline{b_{13}})}++b_{70}(b_{16}+\overline{b_{13}})e^{-(b_{16}+\overline{b_{13}})}+b_{71}(b_{16}+\overline{b_{12}})e^{-(b_{16}+\overline{b_{12}})}+$$
$$+b_{72}(b_{12}+\overline{b_{15}})e^{-(b_{12}+\overline{b_{15}})}+b_{73}(b_{13}+\overline{b_{15}})e^{-(b_{13}+\overline{b_{15}})}+b_{74}(b_{12}+\overline{b_{16}})e^{-(b_{12}+\overline{b_{16}})}+$$
$$+b_{75}(b_{13}+\overline{b_{16}})e^{-(b_{13}+\overline{b_{16}})}+b_{76}\overline{b_{15}}e^{-\overline{b_{15}}}+b_{77}\overline{b_{16}}e^{-\overline{b_{16}}}+b_{78}b_{15}e^{-b_{15}}+b_{79}b_{16}e^{-b_{16}}\Big]\Big\}. \tag{3.25}$$

Where, the over line (bar) represents the conjugate of that particular quantity and the notations/symbols involved in the above solution sets are presented in Appendix.

4. Results and discussion

The hydro magnetic unsteady 2 liquid plasma flow with Hall currents in a horizontal parallel infinite conducting porous plate under a transverse applied magnetic field is researched. The governing equations were determined for velocity and temperature in the case when porous plates are created by conducting materials. Relating computational esteem for different arrangements of estimations of the components included was resolved to speak to their profiles, and these have shown up in Figs. 1-20. For simplicity, we fix the parameters $\sigma_{01}=1.2$, $\sigma_{02}=1.5$ and the viscosity and magnetic permeability are equal, that is, magnetic Prandtl number $=1$, i.e., $P_{r1}=1=P_{r2}$ in all calculations and investigated the impact of other essential parameters. However, it is clear that the solutions rely on the proportion of electron-pressure to the total pressure '*s*'. It is noticed that the analyses in this article and the investigation by L. Raju and Venkat [39] for non-porous plates $(\lambda=0)$ are identical. Also, when there is no rotation and the plates are comprised of non-porous material for a steady motion, this study agrees with that of L. Raju [35]. In the diagrams, the distributions for unsteady motion in the present investigation are shown as solid lines, while the steady motion is represented by dotted lines. Additionally, steady-state variables are marked with an asterisk (*) in all figures. The influence of flow characteristics on the thermal and velocity fields is also analysed and discussed.

The selection of parameter values for the numerical analysis is carefully justified based on their physical significance, practical relevance to magneto hydrodynamic two-fluid plasma flow systems, and alignment with established research in the field. The Hartmann number (*M*) is chosen to represent a range of

magnetic field strengths affecting the flow, corresponding to conditions found in fusion reactors, plasma jets, and geothermal systems where magnetic control plays a vital role [1-3]. The Hall parameter (m) is selected to capture the effect of Hall currents, which are significant in highly ionized plasma under strong magnetic fields, as thoroughly addressed in both classical MHD literature and recent studies [1-2] and [4]. The porosity parameter (λ) reflects realistic scenarios involving permeable conducting plates, influencing fluid flow and heat transfer in applications such as MHD power generators and nuclear system cooling [5]. The Taylor number (K) is set to match rotation rates typically observed in astrophysical and engineering plasma systems, ensuring accurate representation of Coriolis effects [6-7]. Ratios of viscosities, thermal conductivities, electrical conductivities, and height ratios are chosen based on the properties of commonly used liquid metals and two-fluid configurations reported in prior works [8]. These parameter ranges are selected to comprehensively represent the combined effects of electromagnetic forces, rotation, and porosity in two-fluid MHD flows, offering valuable insights for both theoretical understanding and practical engineering applications. Consequently, the chosen parameters are rooted in physical realism, prior literature benchmarks, and the objective of exploring critical regimes governing heat and momentum transfer in rotating MHD plasma channels with permeable conducting plates [1-8]. The results presented in this study illustrate the complex interplay of magnetic, rotational, and porous effects on unsteady two-phase MHD plasma flow and thermal distributions within a horizontal channel bounded by conducting porous plates.

When the ionization parameter $s = 0$:

Figure 1 demonstrates that increasing the Hartmann number M, which represents the strength of the applied magnetic field, leads to a decrease in the temperature distribution in region I, while in region II the temperature initially decreases up to $M=4$, then rises until $M=10$, before falling again. This nonlinear behaviour is due to the competing influences of magnetic damping and Hall current induction in electrically conducting fluids. Physically, a stronger magnetic field suppresses the fluid motion via Lorentz forces, thereby reducing convective heat transfer in some regions while altering induced currents that can locally enhance temperatures.

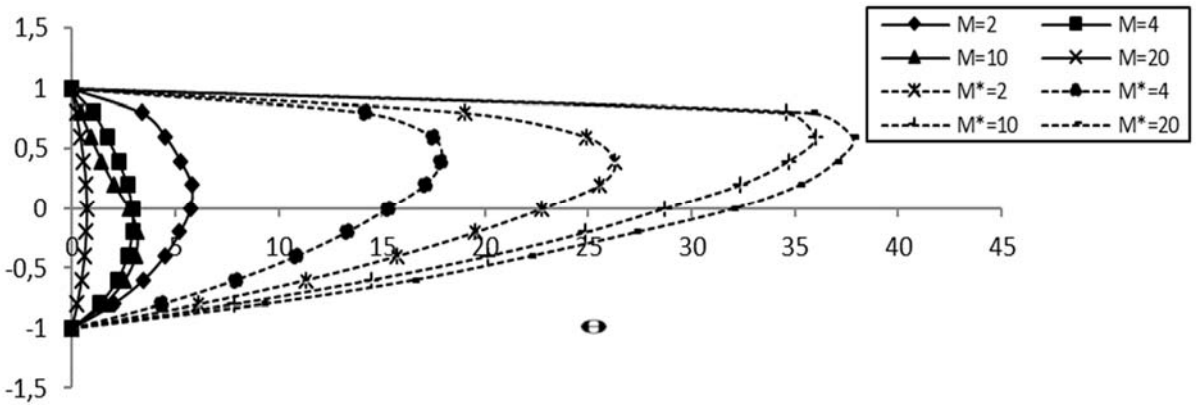

Fig.1. Temperature distribution $\left(\theta_1, \theta_2, \theta_1^*, \theta_2^*\right)$ under varying Hartmann number M with fixed parameters $\lambda = 2$, $m = 2$, $\alpha = 0.333$, $h = 0.75$, $\sigma_0 = 2$, $\sigma_1 = 1.2$, $\sigma_2 = 1.5$, $K = 1$, $\beta = 1$, $\varepsilon = 0.5$, $\rho = 1$, $\omega = 1$, $t = \pi / \omega$ and $s = 0$.

Figure 2 shows the effect of the Hall parameter (m) on thermal fields, where an increase in m causes temperature reductions in both fluid regions. This reduction arises because the Hall effect modifies current paths, enhancing magnetic damping and Coriolis forces associated with rotation, which collectively inhibit flow and heat transport. This illustrates the physical importance of Hall currents in controlling thermal management in plasma flows under strong magnetic and rotational influences.

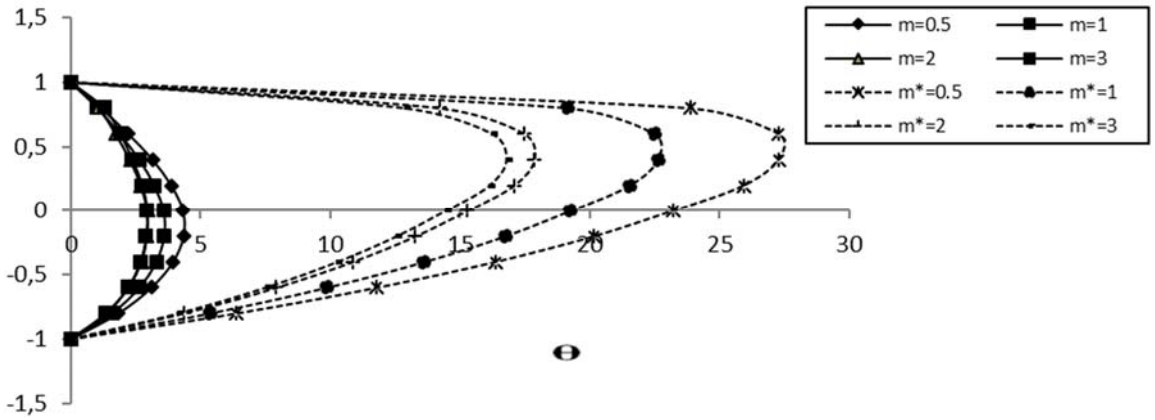

Fig.2. Temperature distribution $\left(\theta_1,\theta_2,\theta_1^*,\theta_2^*\right)$ under varying Hall parameter *m* with fixed parameters $\lambda = 2$, $M = 4$, $\alpha = 0.333$, $h = 0.75$, $\sigma_0 = 2$, $\sigma_1 = 1.2$, $\sigma_2 = 1.5$, $K = 1$, $\beta = 1$, $\varepsilon = 0.5$, $\rho = 1$, $\omega = 1$, $t = \pi/\omega$ and $s = 0$.

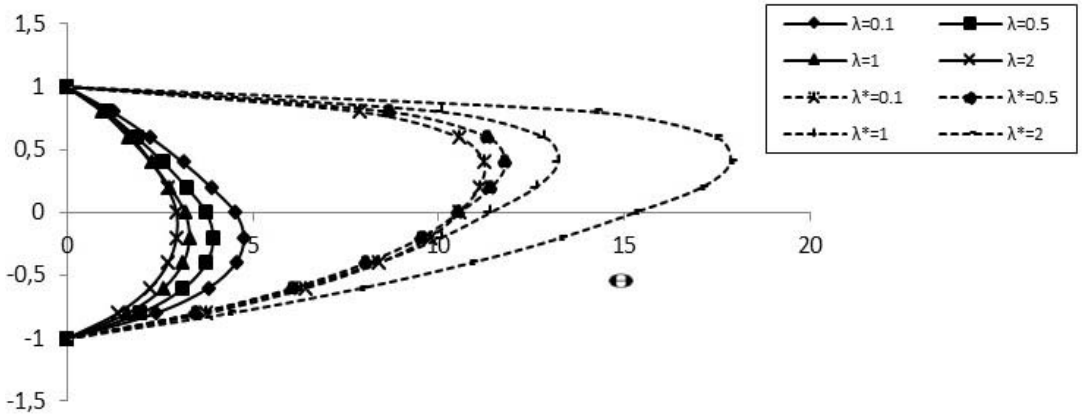

Fig.3. Temperature distribution $\left(\theta_1,\theta_2,\theta_1^*,\theta_2^*\right)$ under varying Porous parameter λ with fixed parameters $m = 2$, $M = 4$, $\alpha = 0.333$, $h = 0.75$, $\sigma_0 = 2$, $\sigma_1 = 1.2$, $\sigma_2 = 1.5$, $K = 1$, $\beta = 1$, $\varepsilon = 0.5$, $\rho = 1$, $\omega = 1$, $t = \pi/\omega$ and $s = 0$.

Figure 3 illustrates the influence of the porosity parameter on the temperature field. As the value of λ increases, the thermal profile in region I decrease, while in region II it first reduces up to $\lambda = 1$ and then starts to rise. With further growth of λ, the heat distribution within the channel tends to shift upward toward the central axis, gradually extending into region I**.** That is, changing the porous nature of the channel plates affect how easily fluid can pass through or interact with them. In some regions, greater permeability lets the fluid move more freely, boosting temperature, while in others it increases resistance and slows the flow. This uneven change across the regions shifts where the maximum temperature occurs. The porosity parameter λ, revealing that increased wall permeability decreases thermal profiles in region I but exhibits a non-monotonic behaviours in region II. Physically, higher porosity allows easier fluid penetration through plates, altering velocity profiles and thermal conduction pathways. The shifting of peak temperatures towards the channel's centreline indicates redistribution of heat transfer zones due to modified flow resistance near porous boundaries, crucial for engineering porous materials in thermal systems.

Figure 4 presents the effect of the Taylor number (*K*), representing the rotational component, on the temperature distribution across the two liquid regions. The results show that as *K* increases, the thermal field in both zones decreases. The Coriolis forces generated by rotation suppress flow velocities and thereby reduce convective heat transfer rates. This result physically underscores the necessity to account for rotational dynamics in the design of plasma and liquid metal flow devices subjected to angular motions.

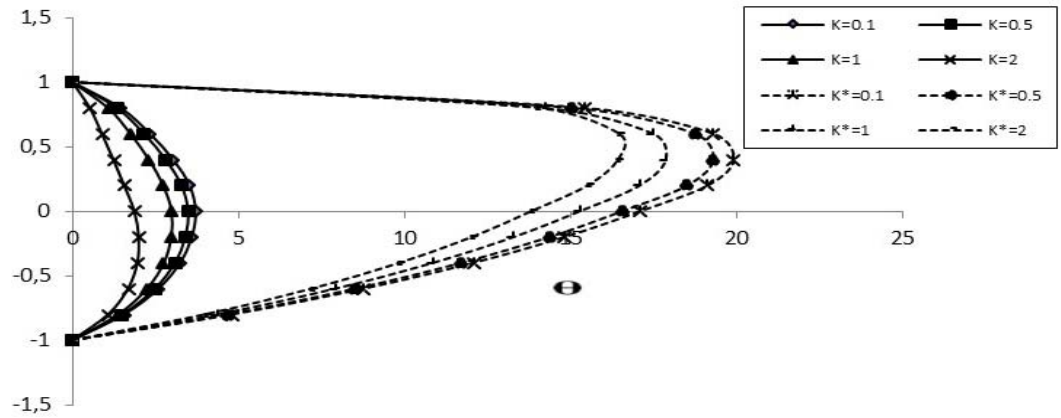

Fig.4. Temperature distribution $\left(\theta_1,\theta_2,\theta_1^*,\theta_2^*\right)$ under varying Taylor number K with fixed parameters $m = 2$, $M = 4,\ \lambda = 2,\ \alpha = 0.333,\ h = 0.75,\ \sigma_0 = 2,\ \sigma_1 = 1.2, \sigma_2 = 1.5,\ \beta = 1, \varepsilon = 0.5,\ \rho = 1,\ \omega = 1,\ t = \pi/\omega$ and $s = 0$.

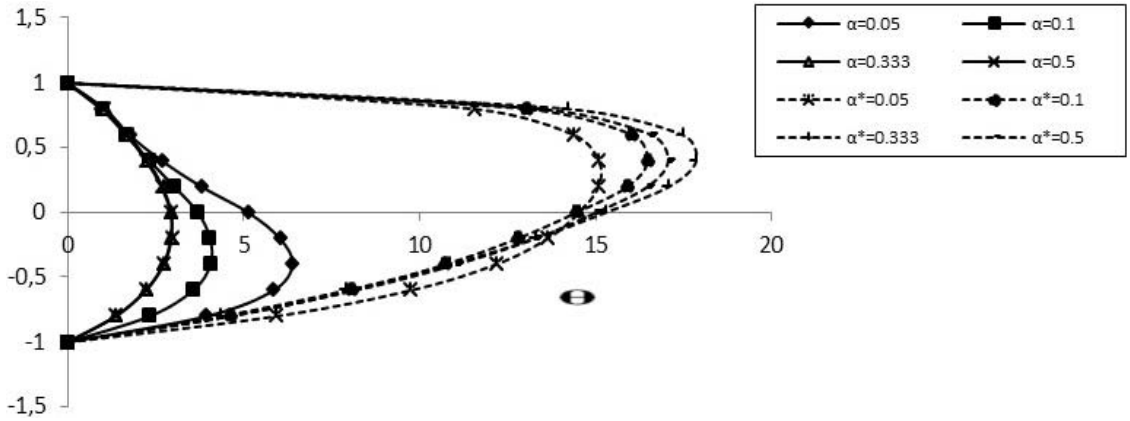

Fig.5. Temperature distribution $\left(\theta_1,\theta_2,\theta_1^*,\theta_2^*\right)$ under varying viscosity ratio α with fixed parameters $m = 2$, $M = 4,\ \lambda = 2,\ h = 0.75,\ \sigma_0 = 2,\ \sigma_1 = 1.2,\ \sigma_2 = 1.5,\ K = 1,\ \beta = 1,\ \varepsilon = 0.5,\ \rho = 1,\ \omega = 1,\ t = \pi/\omega$ and $s = 0$.

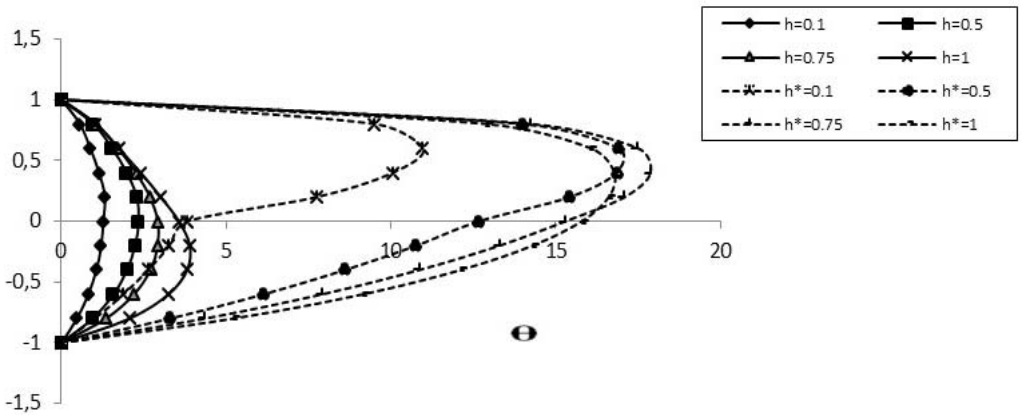

Fig.6. Temperature distribution $\left(\theta_1,\theta_2,\theta_1^*,\theta_2^*\right)$ under varying height ratio h with fixed parameters $m = 2$, $M = 4,\ \lambda = 2,\ \alpha = 0.333,\ \sigma_0 = 2,\ \sigma_1 = 1.2,\ \sigma_2 = 1.5,\ K = 1,\ \beta = 1,\ \omega = 0.5,\ \rho = 1,\ \omega = 1,\ t = \pi/\omega$ and $s = 0$.

Figure 5 depicts the influence of the viscosity ratio parameter α on the temperature field. It is evident that as α increases, the thermal distribution in both regions decreases. Figure 6 illustrates the role of the height ratio h; here, a rise in 'h' leads to an enhancement of the thermal profiles across both zones. Higher viscosity contrasts increase momentum diffusivity differences between fluids, diminishing convective heat transfer, whereas increasing channel height enlarges the flow domain, allowing greater temperature gradients to develop. These findings demonstrate the interplay between fluid properties and geometric configurations in determining thermal performance.

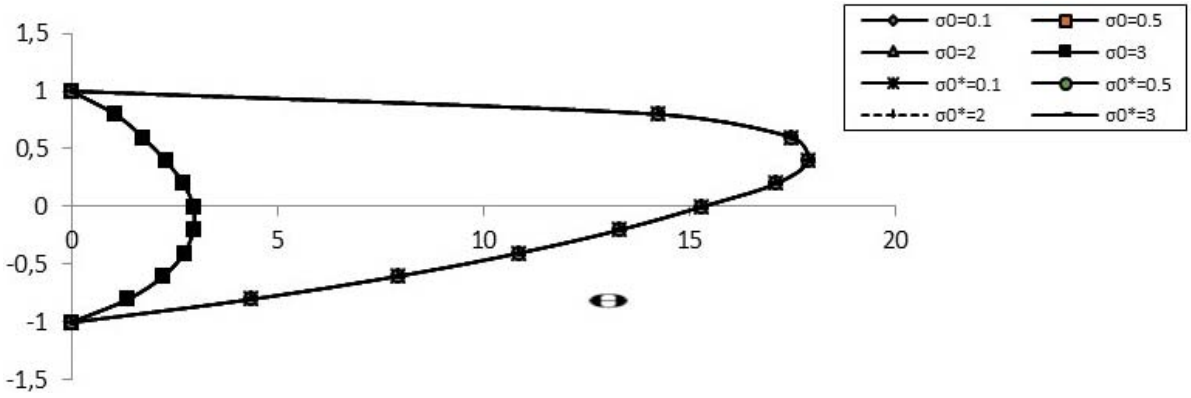

Fig.7. Temperature distribution $\left(\theta_1,\theta_2,\theta_1^*,\theta_2^*\right)$ under varying electrical conductivity ratio σ_0 with fixed parameters $m=2,\ M=4,\ \lambda=2,\ \alpha=0.333,\ h=0.75,\ \sigma_1=1.2,\ \sigma_2=1.5,\ K=1,\ \beta=1,\ \varepsilon=0.5,\ \rho=1,\ \omega=1,$ $t=\pi/\omega$ and $s=0$.

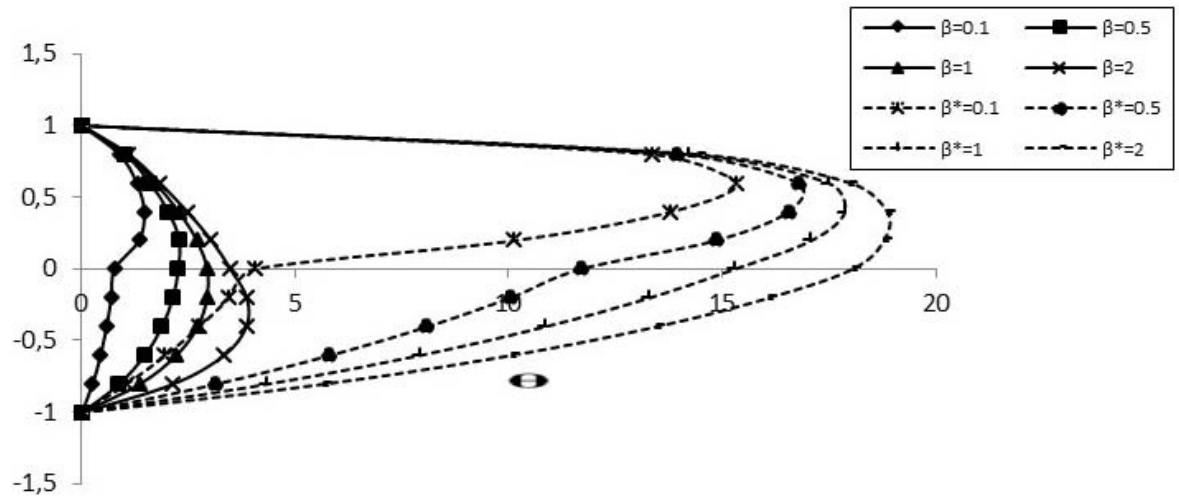

Fig.8. Temperature distribution $\left(\theta_1,\theta_2,\theta_1^*,\theta_2^*\right)$ under varying thermal conductivity ratio β with fixed parameters $m=2,\ M=4,\ \lambda=2,\ \alpha=0.333,\ h=0.75,\ \sigma_0=2,\ \sigma_1=1.2,\ \sigma_2=1.5,\ K=1,\ \varepsilon=0.5,\ \rho=1,$ $\omega=1,\ t=\pi/\omega$ and $s=0$.

Figure 7 depicts the influence of changing the electrical conductivity ratio σ_0 on thermal distributions. The thermal distribution in the two locations does not show any noticeable variation as σ_0 grows. The electrical conductivity ratio changes, suggesting that within considered ranges, electrical conductivity differences between fluids minimally affect temperature fields. Figure 8 illustrates the influence

of the ratio of thermal conductivity β on the heat flow. It shows that an increase in thermal conductivity ratio β elevates temperatures across both zones, affirming the expected physical role of thermal conductivity in facilitating heat diffusion within the fluids.

Figures 9 and 10 present the enhancement of heat transfer coefficients (Nusselt numbers) with increasing Hartmann and Hall parameters. This indicates that stronger magnetic fields and Hall currents improve heat transfer rates at the conducting porous walls, a physically significant insight for optimizing electromagnetic control in thermal management systems involving plasma or liquid metals.

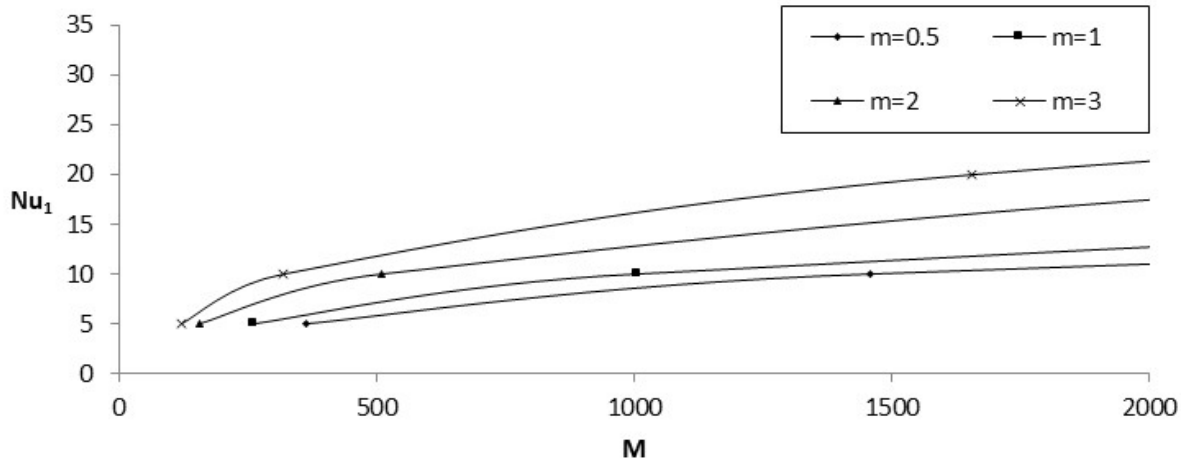

Fig.9. Heat-transfer profiles Nu_1 for varying Hartmann number M with $\lambda = 2$, $\alpha = 0.333$, $h = 0.75$, $\sigma_0 = 2$, $\sigma_1 = 1.2$, $\sigma_2 = 1.5$, $K = 1$, $\varepsilon = 0.5$, $\beta = 1$, $\rho = 1$, $\omega = 1$, $t = \pi / \omega$ and $s = 0$.

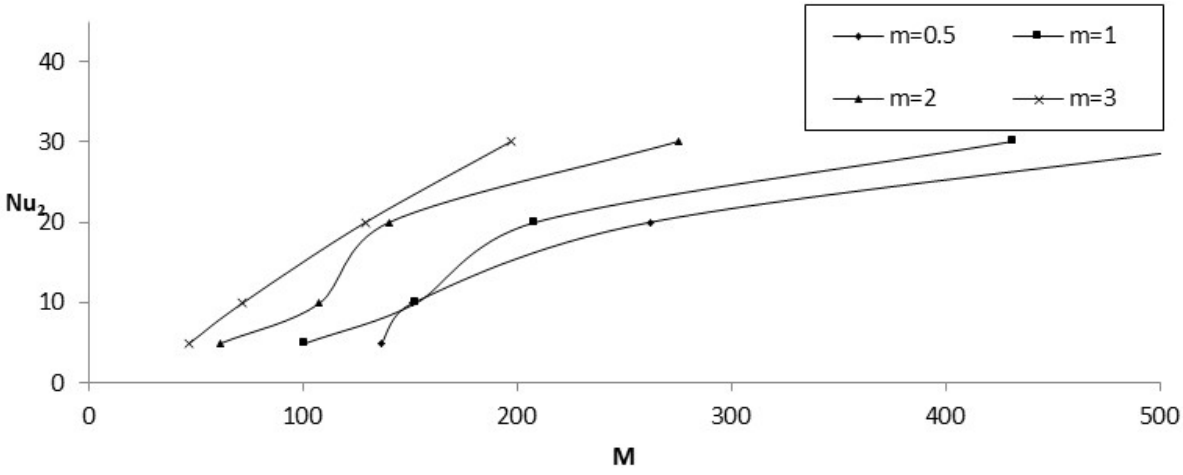

Fig.10. Heat-transfer profiles Nu_2 for varying Hartmann number M with $\lambda = 2$, $\alpha = 0.333$, $h = 0.75$, $\sigma_0 = 2$, $\sigma_1 = 1.2$, $\sigma_2 = 1.5$, $K = 1$, $\varepsilon = 0.5$, $\beta = 1$, $\rho = 1$, $\omega = 1$, $t = \pi / \omega$ and $s = 0$.

When the ionization parameter *s=1/2*:

Figure 11 illustrates the effect of increasing the Hartmann number M on the temperature distribution when the ionization parameter $s = 1/2$. As 'M' increases, the temperature decreases in both fluid regions, reflecting the stronger magnetic field's suppression of fluid motion due to Lorentz forces. This damping effect reduces convective heat transfer, dominating over any Joule heating, thereby uniformly lowering

temperature profiles across the channel. Figure 12 shows the influence of the Hall parameter 'm' on thermal distribution for $s = 1/2$. Rising values of '*m*' continue to cause a drop in temperature in both regions, confirming that Hall currents enhance magnetic damping and rotational Coriolis forces. This results in suppressed flow velocities and diminished heat transfer capacity, important for engineering systems where Hall effects modify plasma flow behaviour.

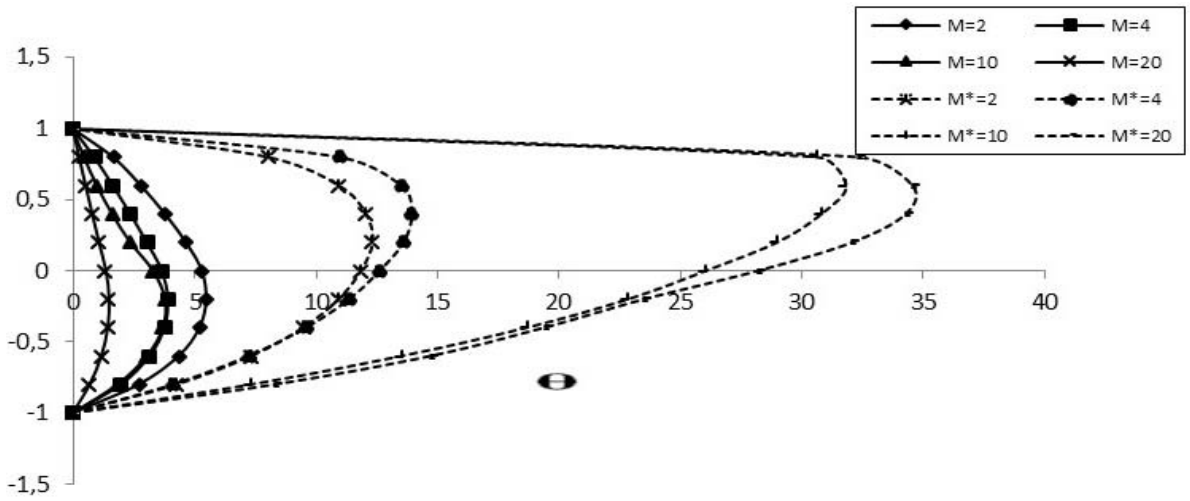

Fig.11. Temperature distribution $\left(\theta_1, \theta_2, \theta_1^*, \theta_2^*\right)$ under varying Hartmann number *M* with fixed parameters $\lambda = 2,\ m = 2,\ \alpha = 0.333,\ h = 0.75,\ \sigma_0 = 2,\ \sigma_1 = 1.2,\ \sigma_2 = 1.5,\ K = 1,\ \beta = 1,\ \varepsilon = 0.5,\ \rho = 1,\ \omega = 1,\ t = \pi/\omega$ and $s = 0.5$.

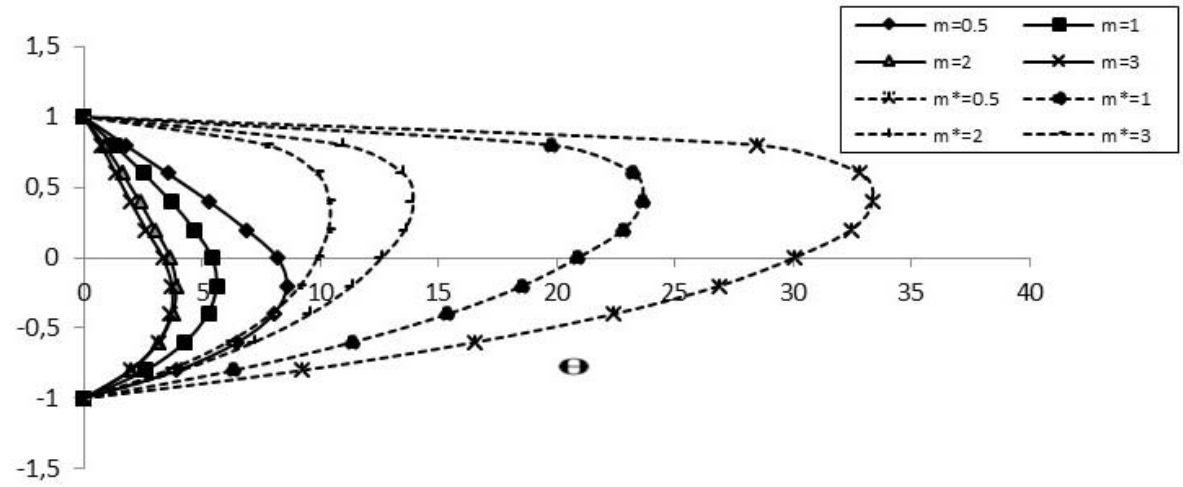

Fig.12. Temperature distribution $\left(\theta_1, \theta_2, \theta_1^*, \theta_2^*\right)$ under varying Hall parameter *m* with fixed parameter $\lambda = 2$, $M = 4, \alpha = 0.333, h = 0.75, \sigma_0 = 2, \sigma_1 = 1.2, \sigma_2 = 1.5, K = 1, \beta = 1, \varepsilon = 0.5, \rho = 1, \omega = 1, t = \pi/\omega$ and $s = 0.5$.

Figure 13 depicts how the porous parameter λ affects the temperature field under $s = 1/2$. As λ increases, temperature decreases in both regions, and the peak temperature gradually shifts upward toward the channel centreline, especially in region I. This indicates complex interactions between wall permeability

and viscous diffusion that influence momentum and heat transport differently in the two fluid layers, highlighting the significance of porous wall design on thermal distribution.

Figure 14 presents the role of the Taylor number '*K*' representing rotation effects on the thermal profiles for $s = 1/2$. An increase in '*K*' decreases temperature levels in both fluid regions. The Coriolis force originating from rotation suppresses fluid motion and convective heat transfer, emphasizing the importance of rotational dynamics in plasma flow control and thermal management.

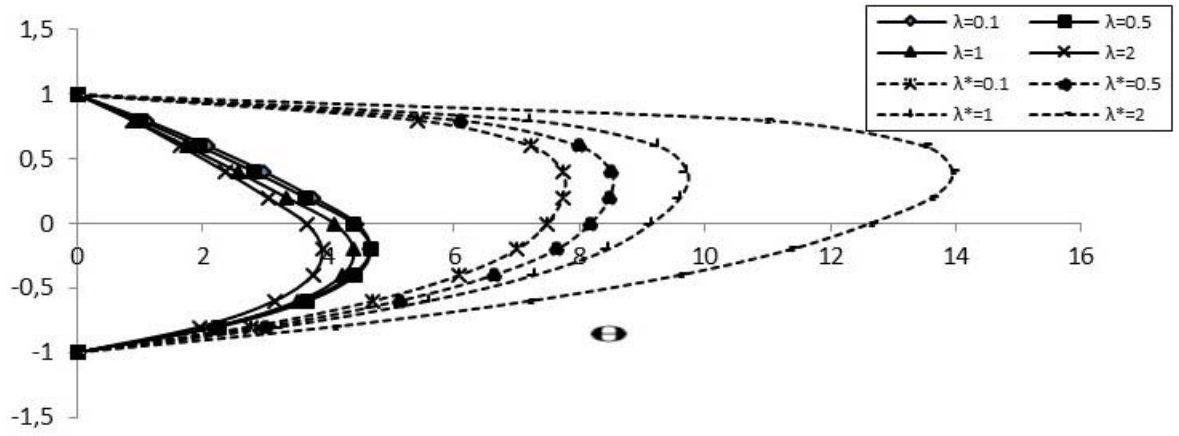

Fig.13. Temperature distribution $\left(\theta_1, \theta_2, \theta_1^*, \theta_2^*\right)$ under varying Porous parameter λ with fixed paramete $m = 2$, $M = 4$, $\alpha = 0.333$, $h = 0.75$, $\sigma_0 = 2$, $\sigma_1 = 1.2$, $\sigma_2 = 1.5$, $K = 1$, $\beta = 1$, $\varepsilon = 0.5$, $\rho = 1$, $\omega = 1$, $t = \pi/\omega$ and $s = 0.5$.

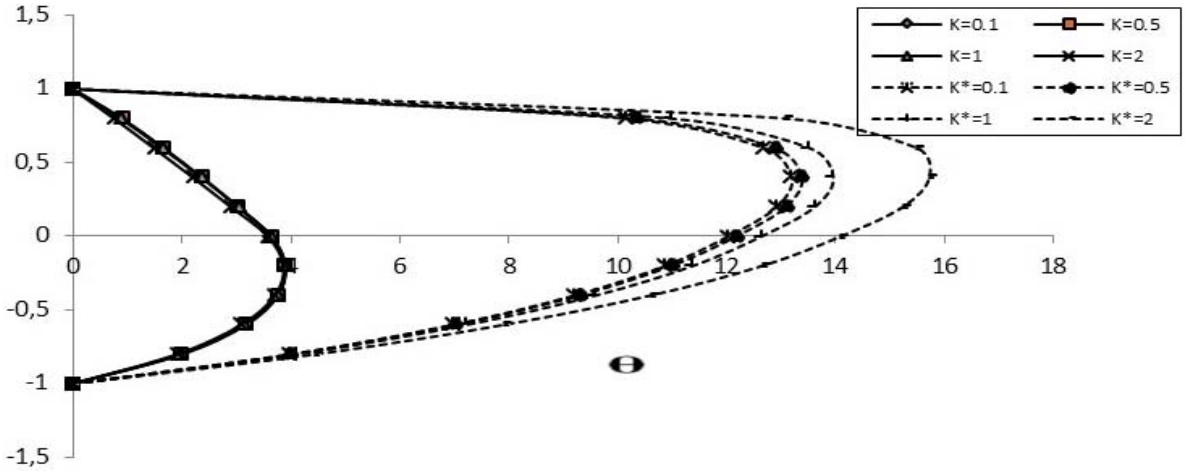

Fig.14. Temperature distribution $\left(\theta_1, \theta_2, \theta_1^*, \theta_2^*\right)$ under varying Taylor number *K* with fixed parameter $m = 2$, $M = 4$, $\lambda = 2$, $\alpha = 0.333$, $h = 0.75$, $\sigma_0 = 2$, $\sigma_1 = 1.2$, $\sigma_2 = 1.5$, $\beta = 1$, $\varepsilon = 0.5$, $\rho = 1$, $\omega = 1$, $t = \pi/\omega$ and $s = 0.5$.

Figure 15 shows the effect of changing viscosity ratio α on temperature distribution when $s = 1/2$. Temperature decreases up to $\alpha = 0.1$ and then raises in region I, whereas in region II it decreases until $\alpha = 0.333$ and then increases. This complex behaviour reflects how variations in fluid viscosities affect viscous dissipation and thermal convection uniquely across fluid layers, underscoring the necessity to consider viscosity contrasts in multi-fluid thermal systems.

Figure 16 illustrates how increasing the height ratio '*h*' enhances thermal profiles in both regions for $s = 1/2$. A larger height ratio increases the flow domain size, allowing more pronounced temperature

gradients and heat transfer effects to develop, which is critical for scaling and designing channels in thermal systems involving multi-phase MHD flows.

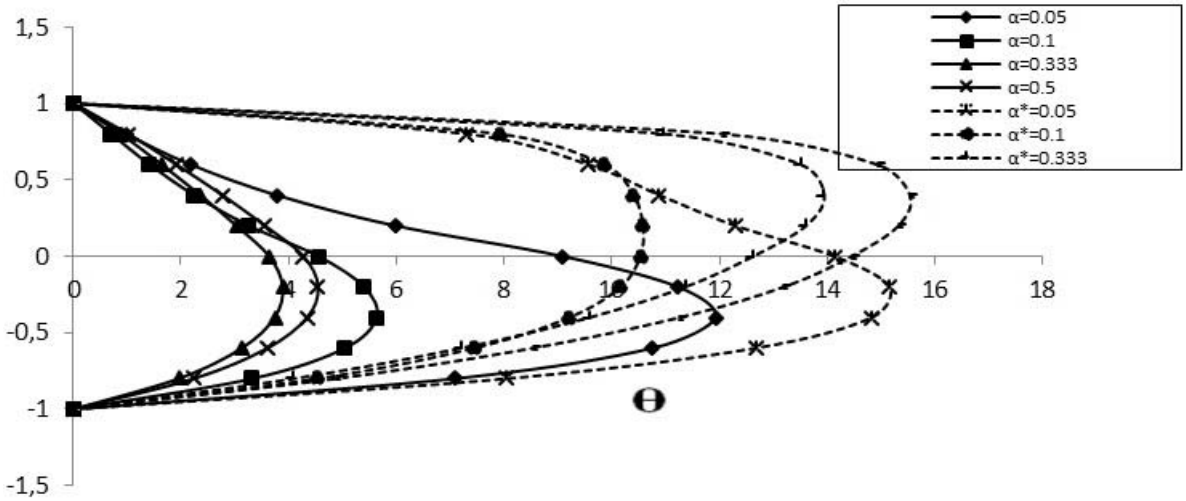

Fig.15. Temperature distribution $\left(\theta_1,\theta_2,\theta_1^*,\theta_2^*\right)$ under varying viscosity ratio α with fixed parameter $m=2$, $M=4$, $\lambda=2$, $h=0.75$, $\sigma_0=2$, $\sigma_1=1.2$, $\sigma_2=1.5$, $K=1$, $\beta=1$, $\varepsilon=0.5$, $\rho=1$, $\omega=1$, $t=\pi/\omega$ and $s=0.5$.

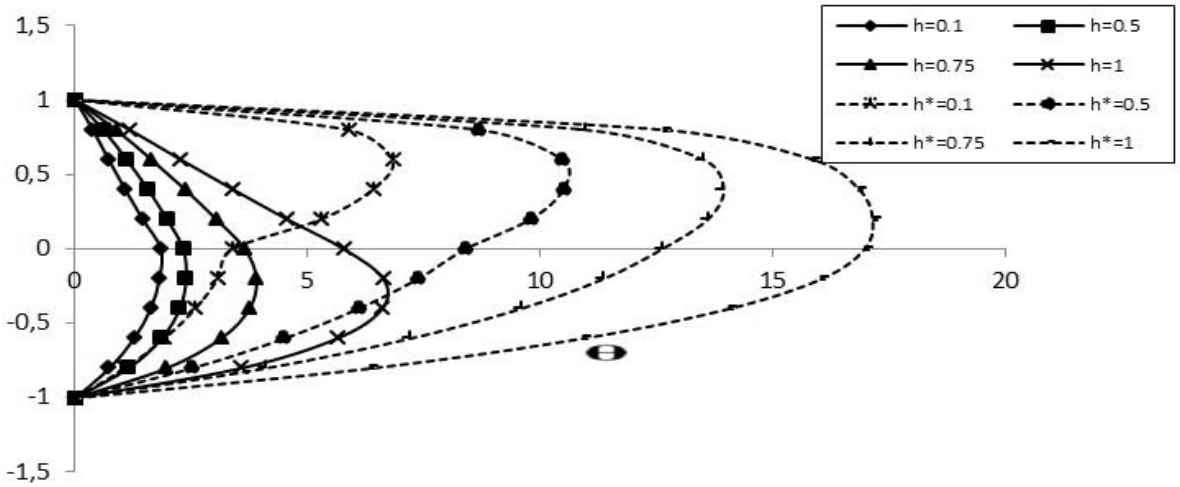

Fig.16. Temperature distribution $\left(\theta_1,\theta_2,\theta_1^*,\theta_2^*\right)$ under varying height ratio h with fixed parameters $m=2$, $M=4$, $\lambda=2$, $\alpha=0.333$, $\sigma_0=2$, $\sigma_1=1.2$, $\sigma_2=1.5$, $K=1$, $\beta=1$, $\omega=0.5$, $\rho=1$, $\omega=1$, $t=\pi/\omega$ and $s=0.5$.

Figure 17 shows the impact of electrical conductivity ratio σ_0 on temperature distribution for $s=1/2$. Temperature in region I rises with σ_0, while in region II it first decreases and then increases after a certain value $\sigma_0=2$. This pattern highlights how electrical conductivity differences between fluids influence Joule heating and magnetic damping nonlinearly, affecting local heat generation and flow suppression differently in the two zones.

Figure 18 presents the effect of thermal conductivity ratio β on temperature distribution, revealing that increasing β enhances temperatures in both fluid regions for $s=1/2$. This behaviour confirms that

higher thermal conductivity facilitates heat diffusion, raising overall temperature levels and improving heat transfer efficiency.

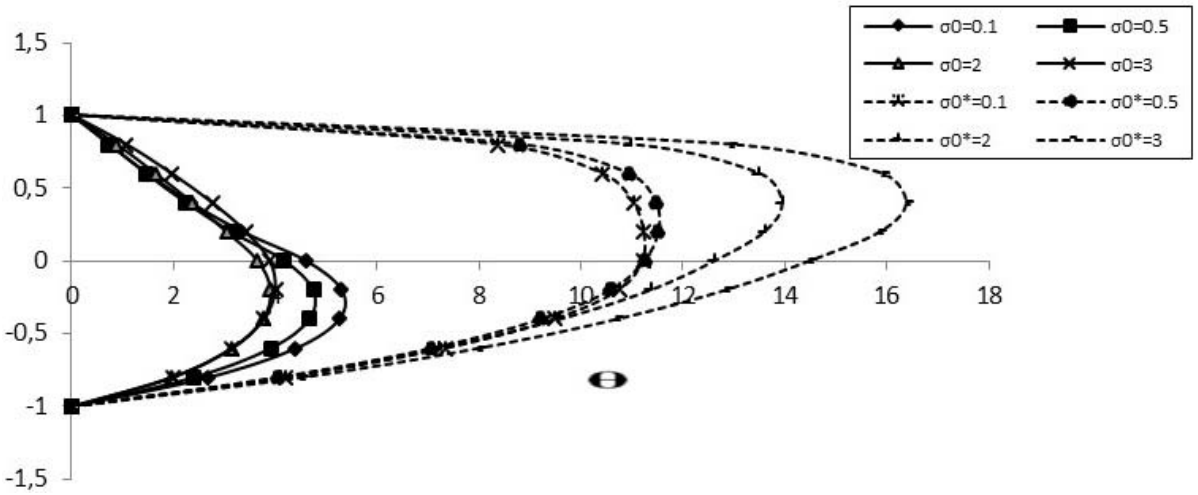

Fig.17. Temperature distribution $\left(\theta_1,\theta_2,\theta_1^*,\theta_2^*\right)$ under varying electrical conductivity ratio σ_0 with fixed parameters $m=2,\ M=4,\ \lambda=2,\ \alpha=0.333,\ h=0.75,\ \sigma_1=1.2,\ \sigma_2=1.5,\ K=1,\ \beta=1,\ \varepsilon=0.5,\ \rho=1,\ \omega=1,$ $t=\pi/\omega$ and $s=0.5$.

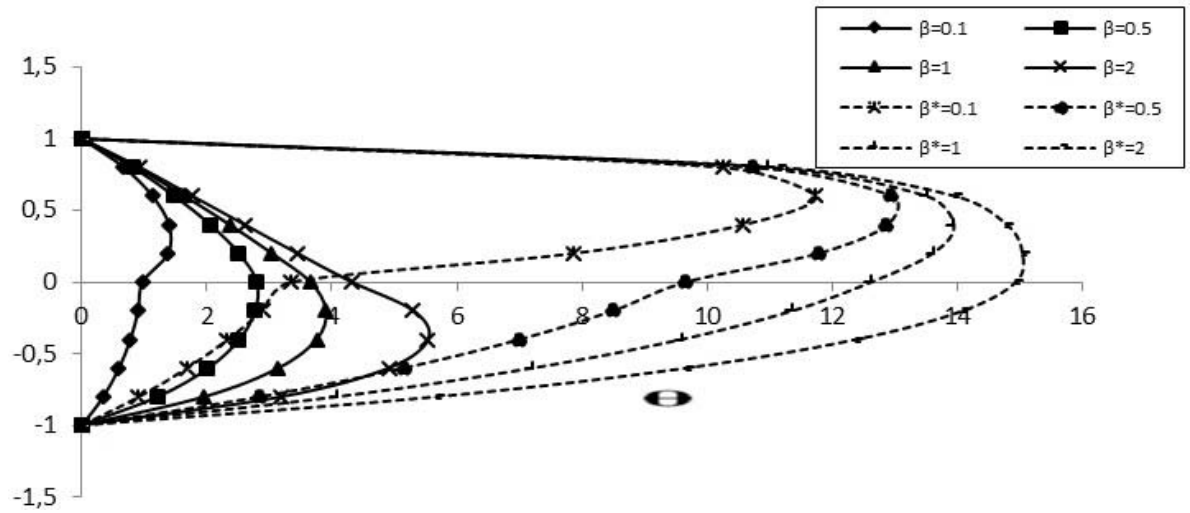

Fig.18. Temperature distribution $\left(\theta_1,\theta_2,\theta_1^*,\theta_2^*\right)$ under varying thermal conductivity ratio β with fixed parameters $m=2,\ M=4,\ \lambda=2,\ \alpha=0.333,\ h=0.75,\ \sigma_0=2,\ \sigma_1=1.2,\ \sigma_2=1.5,\ K=1,\ \varepsilon=0.5,\ \rho=1,$ $\omega=1,\ t=\pi/\omega$ and $s=0.5$.

Figures 19 and 20 show how the heat transfer coefficients (Nusselt numbers) for the two conducting porous plates increase with rising Hartmann number 'M' and Hall parameter 'm' under $s=1/2$. This signifies that stronger magnetic fields and enhanced Hall currents improve the convective heat transfer rates at the boundaries, providing avenues for electromagnetic control to augment thermal management in plasma and liquid metal devices.

Together, Figs 11 to 20 reinforce the physical insights gained for lower ionization parameters, demonstrating the critical roles of magnetic field strength, Hall effects, wall permeability, viscosity contrasts, rotation, and material properties in shaping the thermal and flow characteristics of unsteady MHD two-fluid plasma flows between conducting porous plates.

Overall, the graphical and numerical analyses collectively emphasize the strong sensitivity of unsteady two-phase MHD plasma flow and heat transfer to magnetic field strength, rotation, Hall currents, wall porosity, viscosity, and thermal properties. Understanding these physical interdependencies is vital to predicting system behaviour and achieving optimal control in applications such as fusion reactor cooling, MHD power generation, and advanced propulsion systems.

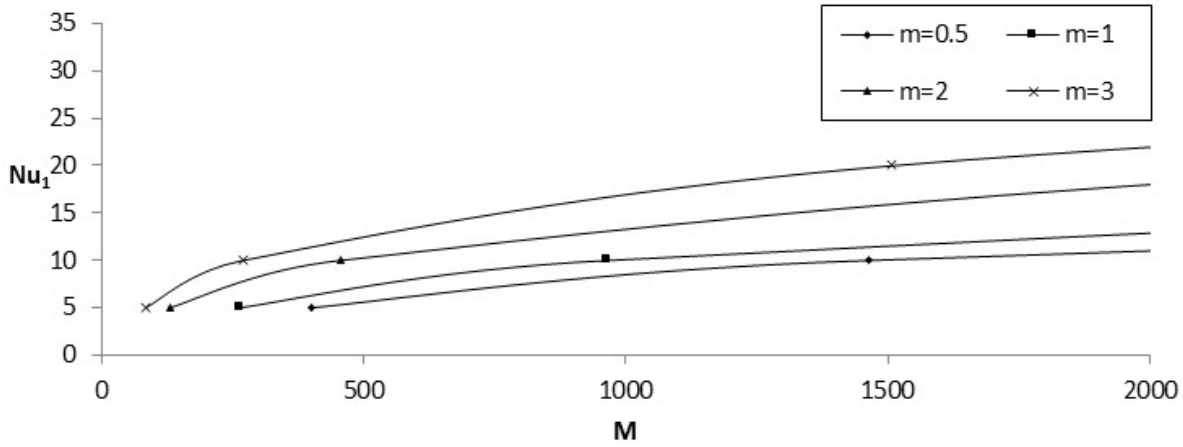

Fig.19. Heat-transfer profiles Nu_1 for varying Hartmann number M with $\lambda = 2$, $\alpha = 0.333$, $h = 0.75$, $\sigma_0 = 2$, $\sigma_1 = 1.2$, $\sigma_2 = 1.5$, $K = 1$, $\varepsilon = 0.5$, $\beta = 1$, $\rho = 1$, $\omega = 1$, $t = \pi / \omega$ and $s = 0.5$.

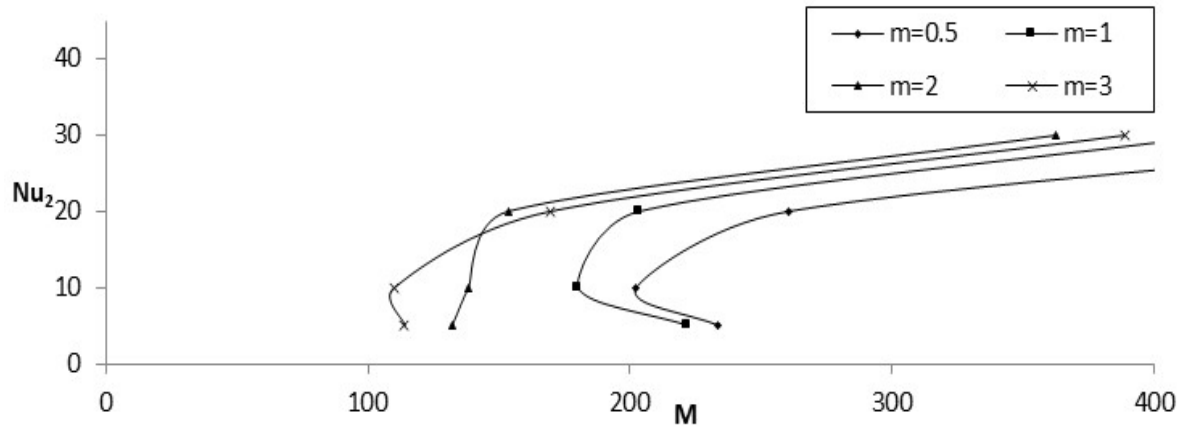

Fig.20. Heat-transfer profiles Nu_2 for varying Hartmann number M with $\lambda = 2$, $\alpha = 0.333$, $h = 0.75$, $\sigma_0 = 2$, $\sigma_0 = 2$, $\sigma_1 = 1.2$, $\sigma_2 = 1.5$, $K = 1$, $\varepsilon = 0.5$, $\beta = 1$, $\rho = 1$, $\omega = 1$, $t = \pi / \omega$ and $s = 0.5$.

5. Validation of results

The present investigation is an extended work of [39] with an inclusion of porosity parameter λ. It is evident that the results of this study agree well with varying Hall parameter on the temperature fields when $\lambda = 0$ (L. Raju and Venkat [39]). This investigation also agrees with that of L. Raju [35] when there is no

impact of rotation and porosity in steady flow ($\lambda = 0$ and $K = 0$).The thick lines in the figures indicate distributions for unsteady motion of the present investigation and the dotted lines represent existing literature (outcomes of without wall porosity/ and rotational component).

6. Conclusion

This study examines how Hall currents influence the unsteady magneto hydrodynamic (MHD) two-layer heat transfer flow in a rotating horizontal channel bounded by two electrically conducting porous plates. Graphs are used to analyse the influence of governing characteristics like the Hartmann number, porous parameter, Hall parameter, rotation parameter, and the ratios of densities, viscosities, and heights, electrical and thermal conductivities on thermal distributions in two fluid zones. The most important findings of this study when the ionization parametric value is zero and half of its estimate are as follows:

i) When ionization parameter $s = 0$

1. Increase in magnetic parameter drops the temperature fields in zone-I, but in zone-II reduces until certain estimated value then rises beyond that estimate thereafter which it decreases again.
2. Raise either in Hall effect or Taylor number or viscosity ratio is to decrease the thermal fields in the two regions.
3. The highest thermal profile within the channel gradually shifts upward from the central axis toward region-I as the porosity parameter increases.
4. The temperature fields are enhanced as the thermal conductivity ratio or height ratio increases.
5. The thermal transfer coefficient rate improves with enhancing range of the Hall parameter and magnetic parameter.

ii) When ionization parameter $s = 1/2$

6. The rise in magnetic parameter, Taylor number, Hall parameter, porous parameter, or viscosity ratio leads to a reduction in the temperature distribution.
7. Thermal profiles become more pronounced as the thermal conductivity ratio or the height ratio increases.
8. In Region I, the temperature profile improves with higher electrical conductivity ratio, whereas in Region II, it decreases up to a certain level before beginning to rise again.
9. The rate of heat transfer coefficient increases with higher values of the magnetic parameter and Hall parameter.

Potential limitations of work, and the future studies

A key limitation of this study is the assumption of perfectly flat interfaces and ideal boundary conditions, which may overlook real-world complexities like interfacial deformation, surface roughness, or instabilities in multiphase flows. Furthermore, the neglect of induced magnetic fields by assuming a low magnetic Reynolds number limits the model's applicability in scenarios involving strong magnetic fields or highly conductive fluids. The chosen parameter ranges were mostly idealized, lacking extensive experimental support. Future research should focus on incorporating dynamic interfaces, non-uniform boundary conditions, and experimental validation. Extending the model to account for nonlinear effects, turbulence, and variable magnetic Reynolds numbers would improve its relevance for practical applications in plasma systems, fusion energy, and advanced MHD technologies.

Acknowledgements

We would like to sincerely thank the anonymous two reviewers and Prof. Pawel Jurczak, Chief-Editor (IJAME) for their great feedback and helpful suggestions - they really helped us make this research better. The authors also, sincerely thank the researchers whose work is cited in this article for their valuable contributions to the field.

Funding

This research was carried out without any financial support from institutions, organizations, government bodies, or external funding sources.

Appendix

$q_1(y,t) = q_{01} + (\varepsilon \cos \omega t)\, q_{11}$ and $q_2(y,t) = q_{02} + (\varepsilon \cos \omega t)\, q_{12}$, where $q_{01} = u_{01} + iw_{01}$, $q_{02} = u_{02} + iw_{02}$,

$q_{11} = u_{11} + iw_{11}$, $q_{12} = u_{12} + iw_{12}$, $\theta_1 = \theta_{01} + (\varepsilon \cos \omega t)\, \theta_{11}$, $\theta_2 = \theta_{02} + (\varepsilon \cos \omega t)\, \theta_{12}$,

$$P_1 = 1 - \frac{m^2 s}{1+m^2},\ P_2 = \frac{-ms}{1+m^2},\ P_3 = 1 - \left(1 - \frac{\sigma_0 \sigma_1}{1+m^2}\right)s,\ P_4 = \frac{-\sigma_0 \sigma_2 ms}{1+m^2},$$

$$b_1 = P_1 + iP_2,\ b_2 = \left(\frac{1-mi}{1+m^2}\right)M^2 - 2iK^2,\ b_3 = -b_1,\ b_4 = P_3 + iP_4,\ b_5 = \left\{\frac{(\sigma_1 - i\sigma_2 m)\alpha h^2 M^2}{1+m^2} - 2ih^2 K^2 \rho\alpha\right\},$$

$$b_6 = -b_4 \alpha h^2,\ b_7 = \frac{\lambda + \sqrt{\lambda^2 + 4b_2}}{2},\ b_8 = \frac{\lambda - \sqrt{\lambda^2 + 4b_2}}{2},\ b_9 = \frac{b_3}{b_2},\ b_{10} = \frac{\lambda + \sqrt{\lambda^2 - 4(\omega \tan \omega t - b_2)}}{2},$$

$$b_{11} = \frac{\lambda + \sqrt{\lambda^2 - 4(\omega \tan \omega t - b_2)}}{2},\ b_{12} = \frac{\lambda_1 + \sqrt{\lambda_1^2 + 4b_5}}{2},\ b_{13} = \frac{\lambda_1 - \sqrt{\lambda_1^2 + 4b_5}}{2},\ b_{14} = \frac{b_6}{b_5},$$

$$b_{15} = \left(b_8 - \frac{b_{12}}{\alpha h}\right)\left(1 - \frac{e^{b_7}}{e^{b_8}}\right) + b_7 - b_8,\ b_{16} = \left(b_8 - \frac{b_{13}}{\alpha h}\right)\left(1 - \frac{e^{b_7}}{e^{b_8}}\right) + b_7 - b_8,$$

$$b_{17} = b_8(b_9 - b_{14})\left(1 - \frac{e^{b_7}}{e^{b_8}}\right) - \left(b_9 - b_{14} - \frac{b_9}{e^{b_8}}\right)(b_7 - b_8),\ b_{18} = \left(b_{11} - \frac{b_{15}}{\alpha h}\right)\left(1 - \frac{e^{b_{10}}}{e^{b_{11}}}\right) + b_7 - b_8,$$

$$b_{19} = \left(b_{11} - \frac{b_{16}}{\alpha h}\right)\left(1 - \frac{e^{b_{10}}}{e^{b_{11}}}\right) - (b_{10} - b_{11}),\ b_{20} = \frac{b_{10} - b_{11}}{e^{b_{11}}},\ b_{21} = \frac{1-mi}{1+m^2},\ b_{22} = \frac{S}{M^2}\left(i + \frac{m(1-i)}{1+m^2}\right),$$

$$b_{23} = \frac{i\sigma_0 \sigma_1 + m\sigma_0 \sigma_2}{1+m^2},\ b_{24} = \frac{s\sigma^2{}_0 \sigma_2}{M^2}\frac{m}{1+m^2} - \left(1 - \frac{\sigma_0 \sigma_1}{1+m^2}\right)\frac{is\sigma_0}{M^2},\ b_{25} = b_{21} i,\ b_{26} = -b_{22},\ b_{27} = -b_{24},$$

$$b_{28} = \frac{-p_{r_1}\left[B_1 b_7 \bar{B}_1 \bar{b}_7 + M^2 B_1 b_{25} \bar{B}_1 \bar{b}_{25}\right]}{(b_7 + \bar{b}_7)^2 + \lambda_2 (b_7 + \bar{b}_7)},\ b_{29} = \frac{-p_{r_1}\left(B_1 b_7 \bar{B}_2 \bar{b}_8 + M^2 B_1 b_{25} \bar{B}_2 \bar{b}_{25}\right)}{(b_7 + \bar{b}_8)^2 + \lambda_2 (b_7 + \bar{b}_8)},$$

$$b_{30} = \frac{-p_{r1}\left[B_2 b_8 \bar{B}_1 \bar{b}_7 + M^2 B_2 b_{25} \bar{B}_1 \bar{b}_{25}\right]}{(b_8 + \bar{b}_7)^2 + \lambda_2 (b_8 + \bar{b}_7)},\ b_{31} = \frac{-p_{r1}\left(B_2 b_8 \bar{B}_2 \bar{b}_8 + M^2 B_2 b_{25} \bar{B}_2 \bar{b}_{25}\right)}{(b_8 + \bar{b}_8)^2 + \lambda_2 (b_8 + \bar{b}_8)},$$

$$b_{32}=\frac{-p_{r1}M^2b_{25}B_1(\bar{b}_{26}-\bar{b}_{25}\bar{b}_9)}{(b_7)^2+\lambda_2(b_7)},\quad b_{33}=\frac{-p_{r1}M^2b_{25}B_2(\bar{b}_{26}-\bar{b}_{25}\bar{b}_9)}{(b_8)^2+\lambda_2(b_8)},\quad b_{34}=\frac{-p_{r1}M^2\bar{b}_{25}\bar{B}_1(b_{26}-b_{25}b_9)}{(\bar{b}_7)^2+\lambda_2(\bar{b}_7)},$$

$$b_{35}=\frac{-p_{r1}M^2\bar{b}_{25}\bar{B}_2(b_{26}-b_{25}b_9)}{(\bar{b}_8)^2+\lambda_2(\bar{b}_8)},\quad b_{36}=\frac{-p_{r1}M^2(b_{26}-b_{25}b_9)(\bar{b}_{26}-\bar{b}_{25}\bar{b}_9)}{\lambda_2},\quad b_{37}=\frac{(-\lambda_2+\sqrt{\lambda_2^2-4p_{r1}\omega\tan\omega t})}{2},$$

$$b_{38}=\frac{-\lambda_2-\sqrt{\lambda_2^2-4p_{r1}\omega\tan\omega t}}{2},\quad b_{39}=\frac{-p_{r1}\varepsilon\cos\omega t\left(B_5b_{10}\bar{B}_5\bar{b}_{10}+M^2B_5\bar{B}_5b_{25}\bar{b}_{25}\right)}{(b_{10}+\bar{b}_{10})^2+\lambda_2(b_{10}+\bar{b}_{10})+p_{r1}\omega\tan\omega t},$$

$$b_{40}=\frac{-p_{r1}\varepsilon\cos\omega t\left(B_5b_{10}\bar{B}_6\bar{b}_{11}+M^2B_5\bar{B}_6b_{25}\bar{b}_{25}\right)}{(b_{10}+\bar{b}_{11})^2+\lambda_2(b_{10}+\bar{b}_{11})+p_{r1}\omega\tan\omega t},\quad b_{41}=\frac{-p_{r1}\varepsilon\cos\omega t\left(B_6b_{11}\bar{B}_5\bar{b}_{10}+M^2B_6\bar{B}_5b_{25}\bar{b}_{25}\right)}{(b_{11}+\bar{b}_{10})^2+\lambda_2(b_{11}+\bar{b}_{10})+p_{r1}\omega\tan\omega t},$$

$$b_{42}=\frac{-p_{r1}\varepsilon\cos\omega t\left(B_6b_{11}\bar{B}_6\bar{b}_{11}+M^2B_6\bar{B}_6b_{25}\bar{b}_{25}\right)}{(b_{11}+\bar{b}_{11})^2+\lambda_2(b_{11}+\bar{b}_{11})+p_{r1}\omega\tan\omega t},\quad b_{43}=\frac{-p_{r1}\left(B_1b_7\bar{B}_5\bar{b}_{10}+M^2B_1\bar{B}_5b_{25}\bar{b}_{25}\right)}{(b_7+\bar{b}_{10})^2+\lambda_2(b_7+\bar{b}_{10})+p_{r1}\omega\tan\omega t},$$

$$b_{44}=\frac{-p_{r1}\left(B_1b_7\bar{B}_6\bar{b}_{11}+M^2B_1\bar{B}_6b_{25}\bar{b}_{25}\right)}{(b_7+\bar{b}_{11})^2+\lambda_2(b_7+\bar{b}_{11})+p_{r1}\omega\tan\omega t},\quad b_{45}=\frac{-p_{r1}\left(B_2b_8\bar{B}_5\bar{b}_{10}+M^2B_2\bar{B}_5b_{25}\bar{b}_{25}\right)}{(b_8+\bar{b}_{10})^2+\lambda_2(b_8+\bar{b}_{10})+p_{r1}\omega\tan\omega t},$$

$$b_{46}=\frac{-p_{r1}\left(B_2b_8\bar{B}_6\bar{b}_{11}+M^2B_2\bar{B}_6b_{25}\bar{b}_{25}\right)}{(b_8+\bar{b}_{11})^2+\lambda_2(b_8+\bar{b}_{11})+p_{r1}\omega\tan\omega t},\quad b_{47}=\frac{-p_{r1}\left(B_5\bar{b}_7\bar{B}_1b_{10}+M^2B_5\bar{B}_1b_{25}\bar{b}_{25}\right)}{(\bar{b}_7+b_{10})^2+\lambda_2(\bar{b}_7+b_{10})+p_{r1}\omega\tan\omega t},\quad \lambda_2=p_{r1}\lambda,$$

$$b_{48}=\frac{-p_{r1}\left(B_6\bar{b}_7\bar{B}_1b_{11}+M^2B_6\bar{B}_1b_{25}\bar{b}_{25}\right)}{(\bar{b}_7+b_{11})^2+\lambda_2(\bar{b}_7+b_{11})+p_{r1}\omega\tan\omega t},\quad b_{49}=\frac{-p_{r1}\left(B_5\bar{b}_8\bar{B}_2b_{10}+M^2B_5\bar{B}_2b_{25}\bar{b}_{25}\right)}{(\bar{b}_8+b_{10})^2+\lambda_2(\bar{b}_8+b_{10})+p_{r1}\omega\tan\omega t},\quad \lambda_3=p_{r2}h\rho\alpha\lambda$$

$$b_{50}=\frac{-p_{r1}\left(B_6\bar{b}_8\bar{B}_2b_{11}+M^2B_6\bar{B}_2b_{25}\bar{b}_{25}\right)}{(\bar{b}_8+b_{11})^2+\lambda_2(\bar{b}_8+b_{11})+p_{r1}\omega\tan\omega t},\quad b_{51}=\frac{-p_{r1}M^2(b_{26}-b_{25}b_9)\bar{b}_{25}\bar{B}_5}{(\bar{b}_{10})^2+\lambda_2(\bar{b}_{10})+p_{r1}\omega\tan\omega t},$$

$$b_{52}=\frac{-p_{r1}M^2(b_{26}-b_{25}b_9)\bar{b}_{25}\bar{B}_6}{(\bar{b}_{11})^2+\lambda_2(\bar{b}_{11})+p_{r1}\omega\tan\omega t},\quad b_{53}=\frac{-p_{r1}M^2(\bar{b}_{26}-\bar{b}_{25}\bar{b}_9)b_{25}B_5}{(b_{10})^2+\lambda_2(b_{10})+p_{r1}\omega\tan\omega t},$$

$$b_{54}=\frac{-p_{r1}M^2(\bar{b}_{26}-\bar{b}_{25}\bar{b}_9)b_{25}B_6}{(b_{11})^2+\lambda_2(b_{11})+p_{r1}\omega\tan\omega t},\quad b_{55}=\frac{-p_{r2}\left(\frac{\beta}{\alpha}B_3\bar{B}_3b_{12}\bar{b}_{12}+h^2\sigma\beta M^2b_{23}\bar{b}_{23}B_3\bar{B}_3\right)}{(b_{12}+\bar{b}_{12})^2+\lambda_3(b_{12}+\bar{b}_{12})+p_{r2}\omega\tan\omega t},$$

$$b_{56}=\frac{-p_{r2}\left(\frac{\beta}{\alpha}B_3\bar{B}_4b_{12}\bar{b}_{13}+h^2\sigma\beta M^2b_{23}\bar{b}_{23}B_3\bar{B}_4\right)}{(b_{12}+\bar{b}_{13})^2+\lambda_3(b_{12}+\bar{b}_{13})+p_{r2}\omega\tan\omega t},\quad b_{57}=\frac{-p_{r2}\left(\frac{\beta}{\alpha}B_4\bar{B}_3b_{13}\bar{b}_{12}+h^2\sigma\beta M^2b_{23}\bar{b}_{23}B_4\bar{B}_3\right)}{(b_{13}+\bar{b}_{12})^2+\lambda_3(b_{13}+\bar{b}_{12})+p_{r2}\omega\tan\omega t},$$

$$b_{58}=\frac{-p_{r2}\left(\frac{\beta}{\alpha}B_4\bar{B}_4b_{13}\bar{b}_{13}+h^2\sigma\beta M^2b_{23}\bar{b}_{23}B_4\bar{B}_4\right)}{(b_{13}+\bar{b}_{13})^2+\lambda_3(b_{13}+\bar{b}_{13})+p_{r2}\omega\tan\omega t},\quad b_{59}=\frac{-p_{r2}h^2\sigma\beta M^2(b_{27}-b_{14}b_{23})\bar{b}_{23}\bar{B}_3}{(\bar{b}_{12})^2+\lambda_3(\bar{b}_{12})+p_{r2}\omega\tan\omega t},$$

$$b_{60}=\frac{-p_{r2}h^2\sigma\beta M^2(b_{27}-b_{14}b_{23})\bar{b}_{23}\bar{B}_4}{(\bar{b}_{13})^2+\lambda_3(\bar{b}_{13})+p_{r2}\omega\tan\omega t},\quad b_{61}=\frac{-p_{r2}h^2\sigma\beta M^2(\bar{b}_{27}-\bar{b}_{14}\bar{b}_{23})b_{23}B_3}{(b_{12})^2+\lambda_3(b_{12})+p_{r2}\omega\tan\omega t},$$

$$b_{62}=\frac{-p_{r2}h^2\sigma\beta M^2(\bar{b}_{27}-\bar{b}_{14}\bar{b}_{23})b_{23}B_4}{(b_{13})^2+\lambda_3(b_{13})+p_{r2}\omega\tan\omega t},\quad b_{63}=\frac{-p_{r2}h^2\sigma\beta M^2(b_{27}-b_{14}b_{23})(\bar{b}_{27}-\bar{b}_{14}\bar{b}_{23})}{\lambda_3},$$

$$b_{64}=\frac{-p_{r2}\varepsilon\cos\omega t\left(\frac{\beta}{\alpha}B_7\bar{B}_7b_{15}\bar{b}_{15}+h^2\sigma\beta M^2b_{23}\bar{b}_{23}B_7\bar{B}_7\right)}{(b_{15}+\bar{b}_{15})^2+\lambda_3(b_{15}+\bar{b}_{15})+p_{r2}\omega\tan\omega t},\quad b_{65}=\frac{-p_{r2}\varepsilon\cos\omega t\left(\frac{\beta}{\alpha}B_7\bar{B}_8b_{15}\bar{b}_{16}+h^2\sigma\beta M^2b_{23}\bar{b}_{23}B_7\bar{B}_8\right)}{(b_{15}+\bar{b}_{16})^2+\lambda_3(b_{15}+\bar{b}_{16})+p_{r2}\omega\tan\omega t},$$

$$b_{66}=\frac{-p_{r2}\varepsilon\cos\omega t\left(\frac{\beta}{\alpha}B_8\bar{B}_7b_{16}\bar{b}_{15}+h^2\sigma\beta M^2b_{23}\bar{b}_{23}B_8\bar{B}_7\right)}{(b_{16}+\bar{b}_{15})^2+\lambda_3(b_{16}+\bar{b}_{15})+p_{r2}\omega\tan\omega t},\quad b_{67}=\frac{-p_{r2}\varepsilon\cos\omega t\left(\frac{\beta}{\alpha}B_8\bar{B}_8b_{16}\bar{b}_{16}+h^2\sigma\beta M^2b_{23}\bar{b}_{23}B_8\bar{B}_8\right)}{(b_{16}+\bar{b}_{16})^2+\lambda_3(b_{16}+\bar{b}_{16})+p_{r2}\omega\tan\omega t},$$

$$b_{68}=\frac{-p_{r2}\left(\frac{\beta}{\alpha}B_3\bar{B}_7b_{12}\bar{b}_{15}+h^2\sigma\beta M^2b_{23}\bar{b}_{23}B_3\bar{B}_7\right)}{(b_{12}+\bar{b}_{15})^2+\lambda_3(b_{12}+\bar{b}_{15})+p_{r2}\omega\tan\omega t},\quad b_{69}=\frac{-p_{r2}\left(\frac{\beta}{\alpha}B_3\bar{B}_8b_{12}\bar{b}_{10}+h^2\sigma\beta M^2b_{23}\bar{b}_{23}B_3\bar{B}_8\right)}{(b_{12}+\bar{b}_{16})^2+\lambda_3(b_{12}+\bar{b}_{16})+p_{r2}\omega\tan\omega t},$$

$$b_{70}=\frac{-p_{r2}\left(\frac{\beta}{\alpha}B_4\bar{B}_7b_{13}\bar{b}_{15}+h^2\sigma\beta M^2b_{23}\bar{b}_{23}B_4\bar{B}_7\right)}{(b_{13}+\bar{b}_{15})^2+\lambda_3(b_{13}+\bar{b}_{15})+p_{r2}\omega\tan\omega t},\quad b_{71}=\frac{-p_{r2}\left(\frac{\beta}{\alpha}B_4\bar{B}_8b_{13}\bar{b}_{16}+h^2\sigma\beta M^2b_{23}\bar{b}_{23}B_4\bar{B}_8\right)}{(b_{13}+\bar{b}_{16})^2+\lambda_3(b_{13}+\bar{b}_{16})+p_{r2}\omega\tan\omega t},$$

$$b_{72}=\frac{-p_{r2}\left(\frac{\beta}{\alpha}B_7\bar{B}_3b_{15}\bar{b}_{12}+h^2\sigma\beta M^2b_{23}\bar{b}_{23}B_7\bar{B}_3\right)}{(b_{15}+\bar{b}_{12})^2+\lambda_3(b_{15}+\bar{b}_{12})+p_{r2}\omega\tan\omega t},\quad b_{73}=\frac{-p_{r2}\left(\frac{\beta}{\alpha}B_8\bar{B}_3b_{16}\bar{b}_{12}+h^2\sigma\beta M^2b_{23}\bar{b}_{23}B_8\bar{B}_3\right)}{(b_{16}+\bar{b}_{12})^2+\lambda_3(b_{16}+\bar{b}_{12})+p_{r2}\omega\tan\omega t},$$

$$b_{74}=\frac{-p_{r2}\left(\frac{\beta}{\alpha}B_7\bar{B}_4b_{15}\bar{b}_{13}+h^2\sigma\beta M^2b_{23}\bar{b}_{23}B_7\bar{B}_4\right)}{(b_{15}+\bar{b}_{13})^2+\lambda_3(b_{15}+\bar{b}_{13})+p_{r2}\omega\tan\omega t},\quad b_{75}=\frac{-p_{r2}\left(\frac{\beta}{\alpha}B_8\bar{B}_4b_{16}\bar{b}_{13}+h^2\sigma\beta M^2b_{23}\bar{b}_{23}B_8\bar{B}_4\right)}{(b_{16}+\bar{b}_{13})^2+\lambda_3(b_{16}+\bar{b}_{13})+p_{r2}\omega\tan\omega t},$$

$$b_{76}=\frac{-p_{r2}h^2\sigma\beta M^2(\bar{b}_{27}-\bar{b}_{14}\bar{b}_{23})B_7b_{23}}{(b_{15})^2+\lambda_3b_{15}+p_{r2}\omega\tan\omega t},\quad b_{77}=\frac{-p_{r2}h^2\sigma\beta M^2(\bar{b}_{27}-\bar{b}_{14}\bar{b}_{23})B_8b_{23}}{(b_{16})^2+\lambda_3b_{15}+p_{r2}\omega\tan\omega t},$$

$$b_{78}=\frac{-p_{r2}h^2\sigma\beta M^2(b_{27}-b_{14}b_{23})\bar{B}_7\bar{b}_{23}}{(\bar{b}_{15})^2+\lambda_3\bar{b}_{15}+p_{r2}\omega\tan\omega t},\quad b_{79}=\frac{-p_{r2}h^2\sigma\beta M^2(b_{27}-b_{14}b_{23})\bar{B}_8\bar{b}_{23}}{(\bar{b}_{16})^2+\lambda_3\bar{b}_{16}+p_{r2}\omega\tan\omega t},$$

$$b_{80}=\frac{-\lambda_3+\sqrt{\lambda^2{}_3-4p_{r2}\tan\omega t}}{2},\quad b_{81}=\frac{-\lambda_3-\sqrt{\lambda^2{}_3-4p_{r2}\tan\omega t}}{2}.$$

Nomenclature

$B_1, B_2 \ldots B_7, \ldots$
$b_1, b_2 \ldots b_{35}$ } – symbols/or functional relations

$\bar{B}$ – magnetic flux density

B_0 – uniform magnetic field

$E_{ix}, E_{iz}, (i = 1,2)$ – electric fields in the x- and z-directions

e – electric charge

h – height ratio

h_1 , h_2 – channel heights of the upper and lower regions

$\overline{J}$ – current density

J_{ix}, J_{iz} – current densities in the *x*- and *z*-directions

I_{ix}, I_{iz} $(i = 1,2)$ – dimensionless current densities

K_1, K_2 – two fluids thermal conductivities

K – Taylor number

M – Hartmann number

m – Hall parameter

m_{ix}, m_{iz} – no-dimensional electric fields

N_1, N_2 – symbols used for $N_1 = m_{x_1} + im_{z_1}$ and $N_2 = m_{x_2} + im_{z_2}$

Nu_1, Nu_2 – heat transfer coefficients

P – pressure

p_e – electron pressure

Pr – Prandtl number

$q_1(y,t)$ and $q_2(y,t)$ – velocities in two regions, where $q_1(y,t) = q_{01}(y) + \varepsilon \cos \omega t \, q_{11}(y)$

$q_2(y,t) = q_{02}(y) + \varepsilon \cos \omega t \, q_{12}(y)$

$q_{01}, q_{02}, q_{11}, q_{12}$ – complex notations of velocities, $q_{01} = u_{01} + iw_{01}$, $q_{02} = u_{02} + iw_{02}$,

$q_{11} = u_{11} + iw_{11}$, $q_{12} = u_{12} + iw_{12}$

q_{m_1}, q_{m_2} – complex form of the mean velocities

s – $= pe / p$ (ratio of electron pressure to the total pressure)

t – time

T – temperature

T_{w_1}, T_{w_2} – temperature at lower and upper plates

u_1 , u_2 – initial velocity distributions in the two regions

u_{m_1}, u_{m_2} – initial mean velocity distributions

$u_{01}(y), u_{02}(y)$ – initial velocity distributions in the steady-state case in two regions

$u_{11}(y), u_{12}(y)$ – transient primary velocities in the two regions

u_p – characteristic velocity $= \left(-\frac{\partial p}{\partial x} \frac{h_i^2}{\mu_i} \right)$, $i = 1,2$

w_1 , w_2 – secondary velocity dispersals in the two regions

w_{m_1}, w_{m_2} – secondary mean velocity dispersals in the two regions

$w_{01}(y), w_{02}(y)$ – secondary velocity dispersals in the steady-state case

$w_{11}(y), w_{12}(y)$ – transient secondary velocity components

(x, y, z) – space coordinates

α – ratio of viscosities

λ – porous parameter

β – ratio of thermal conductivities

μ_1, μ_2 – viscosities- two fluids

σ_0 – ratio of electrical conductivities

σ_1, σ_2 – modified conductivities parallel and normal to the direction of the electric field

σ_{01}, σ_{02} – electrical conductivities of the two fluids

$\sigma_{11}, \sigma_{12}, \sigma_{21}, \sigma_{22}$ – modified conductivities parallel and normal to the direction of the electric field

ε – amplitude

ϕ – viscous dissipation

Ω – Angular velocity, where $\overline{\Omega} = (0, \Omega, 0)$

ρ – ratio of densities

ρ_0 − free charge density
ρ_1, ρ_2 − densities- two fluids
θ_1, θ_2 − non-dimensional forms of temperature dispersals of the two fluids
$\theta_{01}(y),\ \theta_{02}(y)$ − thermal distributions under the steady state in the two regions
$\theta_{11}(y),\ \theta_{12}(y)$ − temperature dispersals under transient state in the two fluid regions
$\tau,\ \tau_e$ − mean collision time between electron and ion, electron and neutral particles
ω − frequency of oscillation
ω_e −electron's gyration frequency

References

[1] Cowling T.G. (1962): *Magnetohydrodynamics.*−Rep. Prog. Phys.,vol.25, pp.244.

[2] Spitzer L.Jr. (1956): *Physics of Fully Ionized Gases.*–Inter Science Publishers, New York.

[3] Sato H. (1961): *The Hall effect in the viscous flow of ionized gas between parallel plates under transverse magnetic field.*– J. Phys. Soc. Japan., vol.16, No.7, pp.1427-1433. https://doi.org/10.1143/JPSJ.16.1427.

[4] Sutton G.W. and Sherman A. (1965): *Engg. Magnetohydrodynamics.*–New York, McGraw-Hill.

[5] Cramer K.R. and Pai Shih-I. (1973): *Magneto-fluid Dynamics for Engineers and Applied Physicists*.– McGraw-Hill Company.

[6] Ram P.C.(1991): *MHD convectiveflow in a rotating fluid with Hall and ion-slip currents.*– Heat and Mass Transfer, vol.26, No.4, pp.203-205, https://doi.org/10.1007/BF01590249.

[7] Linga Raju T. and Ramana RaoV.V.(1993): *Hall effects on temperature distribution in a rotating ionized hydro magnetic flow between parallel walls.*−Int. J. Engg. Sci., vol.31, No.7, pp.1073-1091.

[8] Takhar H.S, Chamkha A.J. and Nath G. (2002): *MHD flow over a moving plate in a rotating fluid with magnetic field, Hall currents and free stream velocity*.– Int.J.Eng.Sci.,vol.40,No.13, pp.1511-1527, https://doi.org/10.1016/S0020-7225(02)00016-2.

[9] Morley N.B., Malang S. and Kirillov I. (2005):*Thermo-fluid magneto hydrodynamic issues for liquid breeders.*– Fusion Science and Technology, vol.47, pp.488-501,https://doi.org/10.13182/FST05-A733.

[10] Attia H.A. (2006): *Effect of Hall current on the velocity and temperature distributions of Couette flow with variable properties.*– PhysicaA.,vol.371,No.2, pp.195-208,https://doi.org/10.1016/j.physa.2006.03.035.

[11] GhoshS.K., Beg O.A. and Narahari M. (2009): *Hall effects on MHD flow in a rotating system with heat transfer characteristics.*–Mecanica, vol.44, pp.741-765, https://doi.org/10.1007/s11012-009-9210-6.

[12] Jha B.K. and Apere C.A. (2010): *Combined effects of Hall and ion-slip currents on unsteady MHD Couette flows in a rotating system.*– J. Phys. Soc. Japan, vol.79, https://doi.org/10.1143/JPSJ.79.104401.

[13] Siddia S., Hossain M.A. and Gorla R.S.R. (2013):*Hall current effects on magnetohydrodynamic natural convection flow with strong cross magnetic field*.– Int.J. ThermalSciences, vol.71, pp.196-204, https://doi.org/10.1016/j.ijthermalsci.2013.04.016.

[14] Makinde O.D., Iskander T., Mabood F., Khan W.A. and Tshehla M.S. (2016):*MHD Couette-Poiseuille flow of variable viscosity nanofluids in a rotating permeable channel with Hall effects.*–Journal of Molecular Liquids, vol.221, pp.778-787, DOI: 10.1016/j.molliq.2016.06.037.

[15] Das S. and Deka R.K. (2021):*Effects of Hall current and rotation on unsteady MHD Couette flow with heat transfer in a porous medium*.–Journal of Applied Fluid Mechanics, vol.14, No.1, pp.239-250.

[16] Linga Raju T. and Satish P.(2023): *Hall and rotation effects on magneto hydrodynamics two fluids slip flow of ionized gases via parallel conduit.*– Heat Transfer, vol.52,No.7,pp.4829-4856,https://doi.org/10.1002/htj.22909.

[17] Attia H.A. (2009): *Effect of Hall current on the velocity and temperature distributions of Couette flow with variable properties and uniform suction and injection.*– Int. Journal of Computational and Applied Mathematics, vol.28,No.2, pp.195-212, https://doi.org/10.1590/S1807-03022009000200004.

[18] Ahmed N. and Goswami J.K. (2011): *Hall effect on MHD forced convection from an infinite porous plate with dissipative heat in a rotating system.*– Turkish Journal of Physics,vol.35,No.3,pp.293-302, https://doi.org/10.3906/fiz-1008-14.

[19] Das S. and Mandal H.K. and Jana, R.N.(2013): *Hall effects on unsteady rotating MHD flow through porous channel with variable pressure gradient*.–Int. J. Computer Applications,vol.83, No.1,pp.7-18. https://doi.org/10.5120/14410-2492.

[20] Khaled K. and Jaber (2015):*Influence of Hall current and viscous dissipation on MHD convective heat and mass transfer in a rotating porous channel with Joule heating*.– American Journal of Mathematics and Statistics, vol.5, No.5, pp.272-284, https://doi.org/10.5923/j.ajms.20150505.08.

[21] Singh J.K., Begum S.G. and Seth G.S. (2018): *Influence of Hall current and wall conductivity on hydromagnetic mixed convective flow in a rotating Darcian channel.*−Physics of Fluids, vol.30, No.11, pp.113602-1-12,https://doi.org/10.1063/1.5054654.

[22] Linga Raju T. and Valli M.N. (2023): *Unsteady two-fluid flow and heat transfer of conducting fluids in conducting fluids in channels under transverse magnetic field*.–J. Engineering Physics and Thermophysics (JEPTR), Springer Publishers, Scopus, vol.96, No.5, pp.1289, 0062-0125/23/9605-1278, Springer Science+Business Media, LLC.

[23] Das D., Shaw S., Mondal K.K. and Kairi R.R. (2023): *Analyzing the impact of boundary slip and absorption effects on the dispersion of solute in a pulsatile channel flow of Casson fluid under magnetic field*.– European Physical Journal Plus, vol.138, art.372, DOI: 10.1140/epjp/s13360-023-03973-8.

[24] Packham B.A. and Sail R. (1971): *Stratified laminar flow of two immiscible fluids*.– Proc. Camb. Phil. Soc., vol.69, pp.443-448.

[25] Lohrasbi J. and Sahai V. (1988): *Magnetohydrodynamic heat transfer in two phase flow between parallel plates*.– Appl. Sci. Res., vol.45, pp.53-66,https://doi:10.1007/BF00384182.

[26] AbdElmaboud Y., Abdesalam S.I., Mekheimer Kh.S. and Vafai K. (2019): *Electromagnetic flow for two-layer immiscible fluids*.– Eng. Sci. Technol. Int. J., vol.22, No.1, pp.237-248.

[27] Roy A.K. and Shaw S. (2021):*Shear augmented micro vascular solute transport with a two- phase model: Application in nano particle assisted drug delivery*.–Physics of Fluids, vol.33, No.3, art.031904, DOI:10.1063/5.0035754.

[28] Shail R. (1973): *On laminar two-phase flows in magnetohydrodynamics*.− Int. J. Engg. Sci., vol.11, pp.1103-1109, https://doi.org/10.1016/0020-7225(73)90111-0.

[29] Kalra G.L., Kathura S.N., Hosking R.J. and Lister G.G.(1970):*Effect of Hall current and resistivity on the stability of a gas-liquid system*.– Journal of Plasma Physics., vol.4, No.3, pp.451-469,https://doi.org/10.1017/S0022377800005158.

[30] Linga Raju T. and Satish P.(2023): *MHD two liquid plasma heat transfer flow with Hall current between parallel plates*.– International Journal of Applied Mechanics and Engineering,vol.28,No.3, pp.65-85, https://doi.org/10.59441/ijame/172898.

[31] Umavathi J.C., Mateen A., Chamkha A.J. and Al-Mudhaf A. (2006): *Oscillatory Hartmann two-fluid flow and heat transfer in a horizontal channel.*−Int.J.Appl.Mech. and Engg.,vol.11, No.1, pp.155-178.

[32] Linga Raju T. and Nagavalli M. (2014): *MHD two-layered unsteady fluid flow and heat transfer through a horizontal channel between parallel plates in a rotating system.*−Int. J. Appl. Mech. and Engg., vol.19, No.1, pp.97-121, https://doi.org/10.2478/ijame-2014-0008.

[33] Sharma P.R. and Sharma Kalpana (2014): *Unsteady MHD two-fluid flow and heat transfer through a horizontal channel.*−Int. J. of Engineering Science Invention Research and Development., vol.1, No.3, pp.65-72.

[34] Sivakamini L and Govindarajan A. (2019): *Unsteady MHD flow of two immiscible fluids under chemical reaction in a horizontal channel.*−AIP conference proceedings 2112. pp.020157-1 to 9, DOI.org/10.1063/1.5112342. https://doi.org/10.1063/1.5112342.

[35] Linga Raju T.(2019): *MHD heat transfer two-ionized fluids flow between two parallel plates* with *Hall currents.*– Results in Eng., ELSEVIER Scopus Indexed Journal, vol.4, pp.100043,https://doi.org/10.1016/j.rineng.2019.100043.

[36] Linga Raju T.and Satish P.(2023): *Slip regime MHD 2-liquid plasma heat transfer flow with hall currents between parallel.*– Int. J. of Applied Mechanics and Engg., vol.28,No.3, pp.65-85,https://doi.org/ 10.59441/ijame/172898.

[37] Linga Raju T. and Satish P.(2023): *Heat transfer rotating MHD two-liquid slip flow regime with Hall current*.– Heat Transfer.,vol.52, No.7, pp.4640-4661, https://doi.org/10.1002/htj.22900.

[38] Linga Raju T.and Venkata Rao B. (2022): *Unsteady electro magneto hydrodynamic flow and heat transfer of two ionized fluids in a rotating system with Hall currents.*– Int. J. App. Mech. Eng. vol.27, No.1, pp.125-145, https://doi.org/10.2478/ijame-2022-0009.

[39] Linga Raju T. and Venkata Rao B. (2022): *The Hall Effect on MHD 2-Fluid Unsteady Heat Transfer Flow of Plasma in a Rotating System via a Straight Channel Between Conducting Plates.*– Int. J. App. Mech. Eng. vol.27, No.3, pp.137-162. https://doi.org/10.2478/ijame-2022-0041.

[40] Nikodijevic M., Stamenkovic Z., Petrovic J. and Kocic M. (2020): *Unsteady fluid flow and heat transfer through a porous medium in a horizontal channel with an inclined magnetic field.*– Transactions of FAMENA., vol.44, No.4, pp.31-46, DOI:10.21278/TOF.444014420.

[41] Khader M.M. and Ram Prakash Sharma (2021): *Evaluating the unsteady MHD micropolar fluid flow past stretching/shirking sheet with heat source and thermal radiation: Implementing fourth order predictor-corrector FDM*.– Math. and Comp. in Sim., vol.181,pp.333-350, https://doi.org/10.1016/j.matcom.2020.09.014.

[42] Ram Prakash Sharma and Mishra S.R. (2022): *A numerical simulation for the control of radiative heat energy and thermophoretic effects on MHD micropolar fluid with heat source.*–Journal of Ocean Engineering and Science, vol.7, No.1, pp.92-98,https://doi.org/10.1016/j.joes.2021.07.003.

[43] Ram Prakash Sharma and Debasish Gorai (2024): *Unveiling the dynamic symphony of melting heat transfer in the flow between a stretching Riga plate and a squeezing plate.*– Int. Communications in Heat and Mass Transfer, vol.156, article 107565, https://doi.org/10.1016/j.icheatmasstransfer.2024.107565.

[44] Abhishek Sharma and Ram Prakash Sharma (2025): *Utilizing neural networks to illustrate the dynamics of viscous fluid flow over curved surface with homogeneous and heterogeneous reactions.*– Engineering Applications of Artificial Intelligence, vol.159, Part A, https://doi.org/10.1016/j.engappai.2025.111629.

[45] Ram Prakash Sharma, Bimal Kumar Barik, Vinay Kumar V. and Abhishek Sharma (2025): *Illustration of low oscillating magnetic field on sodium alginate-based hybrid nano-fluid flow between two revolving disks: An artificial neural network-based study.*– Engineering App. of Artificial Intelligence, vol.155, https://doi.org/10.1016/j.engappai.2025.111101.

[46] Vinay Kumar V. and Ram Prakash Sharma (2025): *Entropy generation minimization in nuclear reactor cooling via rough rotating disk: a statistical approach.*– Multi Scale and Multidisciplinary Modelling, Experiments and Design, vol.8, No.5, https://doi.org/10.1007/s41939-025-00846-8.

[47] Spitzer Jr. L. (1956): *Physics of Fully Ionized Gases*.– Inter Science Publishers, New York.

Received: February 17, 2025
Revised: November 12, 2025